

X-RAY PRODUCTION IN LOW VELOCITY HEAVY
ION-ATOM COLLISIONS

X-RAY PRODUCTION IN LOW VELOCITY HEAVY
ION-ATOM COLLISIONS

By

WILLIAM RONALD STOTT, B.Sc., M.Sc.

A Thesis

Submitted to the School of Graduate Studies
in Partial Fulfilment of the Requirements
for the Degree
Doctor of Philosophy

©WILLIAM RONALD STOTT 1978

McMaster University

March 1978

DOCTOR OF PHILOSOPHY (1978)
(Physics)

McMASTER UNIVERSITY
Hamilton, Ontario.


TITLE: X-ray Production in Low Velocity Heavy Ion-Atom
Collisions

AUTHOR: William Ronald Stott, B.Sc. (Carleton)
M.Sc. (McMaster)

SUPERVISOR: Dr. J. C. Waddington

NUMBER OF PAGES: xi, 100

SCOPE AND CONTENTS:



ABSTRACT

Two aspects of x-ray production have been studied in the collisions of slow heavy ions with heavy atoms. One part of this study deals with the continuum x-rays produced by the collision of ion beams with gold target atoms while the other part deals with the double K-vacancy production in collisions of 80 MeV iodine beams with atoms of atomic numbers near that of iodine.

Beams of four different ions ranging in atomic number from $Z=6$ (carbon) to $Z=35$ (bromine) and having the same velocity ($v \approx 0.04 c$) bombarded gold atoms to produce very similar radiation continua extending from 20 keV photon energy. The observed radiation continua cannot be explained, in their entirety, as molecular orbital x-rays.

The double K-vacancy production was produced in the bombardment by an iodine beam of seven thin targets ranging from silver to lanthanum. The double vacancies were detected by observing two K x-rays emitted simultaneously using a coincidence technique with solid state detectors. The energy differences of the K x-rays emitted have been determined as well as the nature of the sharing of vacancies between target and projectile atoms. Models for double K-vacancy production considered include the molecular orbital multiple collision approach and the binary encounter formalism of direct Coulomb

excitation. Also a calculation of the double to single K-
vacancy ratios was made using a double L-vacancy multiple
collision MO mechanism in which the double to single L-vacancy
cross section ratio was treated as a free parameter.

ACKNOWLEDGEMENTS

Many people have assisted me in my studies while at McMaster and I wish to offer my thanks to those who have contributed to my work and my education. Without their contributions my stay would not have been as rewarding and fulfilling as it has been.

It is a pleasure to thank the staff of the tandem lab for their assistance in conducting experiments and for giving me a working knowledge of the operation of a high technology laboratory. The target foils for most of the experiments were expertly prepared by Y. Peng. Thank you.

I am grateful to the members of our research group who have spent many long hours assisting in the successful completion of the experiments. Their friendship and friendly banter have been one of the highlights of my McMaster experience.

The coincidence data in this work could not have been analyzed without the use of a computer program written by Doug Petty who graciously allowed me the use of it.

I wish to thank Helen Kennelly for the rapid and expert typing of the thesis manuscript. Also, I gratefully acknowledge Patty Petty for her expert preparation of many of the figures.

Particularly, I am most thankful to my supervisor, Dr. Jim Waddington, who has been the inspiration behind the work.

Many times when researcher enthusiasm was low he has injected new ideas and insights which smoothed the way out of the woods. It is a pleasure to work and to associate with Jim as a friend.

The National Research Council is thankfully acknowledged for financial support of the work.

TO MY FATHER AND MOTHER

TABLE OF CONTENTS

<u>CHAPTER</u>		<u>Page</u>
1	INTRODUCTION	1
2	INNER SHELL VACANCY PRODUCTION	
	2.1 Introduction	4
	2.2 The Molecular Orbital Model	5
	2.3 Molecular Orbital Correlation	10
	2.4 MO Excitation Mechanisms	14
3	EXPERIMENTAL TECHNIQUES	
	3.1 Introduction	21
	3.2 X-ray Continua Techniques	21
	3.3 Double K X-ray Techniques	24
	3.4 Timing and Background Considerations	27
	3.5 X-ray Detectors	32
	3.6 The Iodine 125 Source	33
	3.7 Coincidence Analysis Considerations	35
4	X-RAY CONTINUA EXPERIMENTS	41
5	DOUBLE K-VACANCY STUDIES	
	5.1 Introduction	52
	5.2 Satellite and Hypersatellite Structure	54
	5.3 Energies of the X-rays	60
	5.4 Vacancy Sharing	63
	5.5 Single K-vacancy Production	71
	5.6 Double K-vacancy Production	75
	5.7 Double L-vacancy Production	87
6	SUMMARY	91
	APPENDIX	95
	REFERENCES	96

LIST OF FIGURES

<u>FIGURE</u>		<u>Page</u>
2-1	Regions of validity for various models for inner shell vacancy production	6
2-2	Relativistic 20-electron I-Au correlation diagram	11
2-3	Semi-quantitative MO diagram of Ar-Ar molecule	13
2-4	Schematic MO diagram for case $Z_1 \gg Z_2$	15
2-5	MO diagram for near resonance of L and K orbitals of target and projectile atoms	16
2-6	Schematic MO diagram for case Z_1 slightly greater than Z_2	17
3-1	Schematic of electronics of continuum experiments	23
3-2	Schematic of double vacancy experimental arrangement	25
3-3	Photograph of x-ray coincidence chamber	26
3-4	Schematic of electronics of double vacancy studies	28
3-5	TAC spectrum of iodine on indium experiment	31
3-6	The absolute efficiencies of the three detectors used	34
3-7	X-ray spectrum of ^{125}I source	36
3-8	Si(Li) detector projection of x-rays from iodine on indium experiment	37
3-9	Ge(Li) detector projection of x-rays from iodine on indium experiment	38

<u>FIGURE</u>		<u>Page</u>
4-1	Unnormalized spectra from continuum experiments	44
4-2	Angular distribution of 20-22 keV continuum x-rays	49
5-1	The Si(L1) chance spectra and the $K_{\alpha}^s + K_{\alpha}^h$ gated coincidence spectra of iodine on indium experiment	57
5-2	The Si(Li) coincidence spectra of the K_{α}^s and the K_{α}^h gates of the iodine on indium experiment	59
5-3	Schematic representation of possible x-ray coincidences from double vacancies	61
5-4	Schematic MO correlation diagram illustrating W_{2p} and W_{1s} vacancy sharing processes	66
5-5	Plot of ratios of target to projectile single K-vacancies versus parameter x .	67
5-6	Plot of the ratios of target to projectile double K-vacancy coincidence events as a function of x .	70
5-7	Summed target and projectile K-vacancy cross sections for 62 MeV iodine for collisions in region of symmetry	72
5-8	Ratio of double K-vacancies to single K-vacancies versus target Z for 80 MeV iodine projectiles	77
5-9	Schematic MO correlation diagram illustrating $2p_{1/2} - 2p_{3/2}$ united atom splitting.	84
5-10	Plot of the ratio of double to single K-vacancies as a function of atomic number. The line is a calculation of the ratios using the double L-vacancy calculations assuming $\sigma_{1x}^{2p(2)} / \sigma_{1x}^{2p} = 0.10$.	89

LIST OF TABLES

<u>TABLE</u>		<u>Page</u>
4-1	Photon cross sections from continuum studies	46
5-1	K x-ray line energy differences of coincidence work	64
5-2	Calculations of the double K-vacancy cross section components and the single K-vacancy cross section calculations	80

CHAPTER 1
INTRODUCTION

In the early years of this century it was known that heavy elements when struck with energetic alpha particles from radioactive sources would emit characteristic x-rays. However, it was not until 1934 after the advent of linear accelerators that Coates (1934) observed characteristic x-rays from a number of elements when they were bombarded by mercury ions with energies as high as 2.4 MeV. This pioneering work was not only the first to observe inner-shell excitations in heavy ion-atom collisions but Coates also proposed that molecular interactions were responsible for the vacancies that resulted in the x-rays. This idea lay dormant for nearly 30 years until the 1960's when Van de Graaff accelerators became available for the study of heavy ion collisions. Electron excitation in heavy ion-atom collisions plays a very important role in the modern day study of the atom (Richard, 1975).

In the 1960's the fluctuation of K, L and M x-ray production cross sections as a function of target atomic number when bombarded by fission products (Armbruster et al., 1964 and Specht, 1965) brought into focus the value of collision studies using heavy ions. The experimental study and

theoretical development of heavy ion collisions expanded quite dramatically as a consequence of the new developments (e.g. see reviews by Garcia et al., 1973; Kessel and Fastrup, 1973; Hansteen, 1975 and Meyerhof and Taulbjerg, 1977). The study of the enhancement of x-ray production cross sections when target and projectile atomic levels match is now understood in terms of a transient formation of a diatomic molecule (Fano and Lichten, 1965).

A fascinating prediction for molecular K-vacancy formation is that positrons as well as x-rays may be emitted from high-energy heavy-atom collisions such as 1600 MeV uranium on uranium (e.g., Müller, 1976). Positrons may be produced if vacancies exist in an atomic state that is bound by greater than twice the rest mass of the electron. This effect would provide a new experimental test for the theory of quantum electrodynamics. In such an experiment, it is crucial that the interpretation of the x-ray spectra and the formation of K-vacancies be well understood.

This thesis study is broadly divided into two parts, one deals with the study of continuum radiation due to electronic transitions during the collision, the other refers to two vacancy formation in the K-shells of the collision partners that leads to characteristic K x-ray emission once the colliding partners separate. The collisions are considered as low velocity insofar as the projectile velocity ($v_{\text{proj.}} \approx .04c$, in the present study) is much less than the inner-shell electron

orbital velocity ($v_e \sim 0.3 c$, for $Z \approx 50$). Furthermore, if the collision is between particles of approximately equal atomic number, then the vacancy production may be understood in the context of transitory orbitals of a diatomic molecule. The same, however, may not be said if the two are quite disparate in atomic number.

The value of the studies of the continuum radiation produced in heavy ion-atom collisions is that they were the first to be reported between quite asymmetric collision partners. The continua produced appeared quite similar to continua of symmetric collisions which were ascribed to molecular orbital radiation. However, the continua were shown not to be a result of this quasi-molecular process. Greater care was thus shown to be necessary in identifying continuum spectra as resulting from molecular orbital radiation. An interesting aspect of the double vacancy work is the experimental techniques used in the study of double K-vacancy production in heavy ion-atom collisions. These studies have been performed in a different manner than other double vacancy studies in that photon-photon coincidence techniques (well known techniques in nuclear physics) have been used to study collision induced vacancy production. Coincidence studies previously were done using radioactive sources while heavy ion-atom collision x-rays have been studied using crystal spectrometers.

CHAPTER 2

INNER SHELL VACANCY PRODUCTION

2.1 Introduction

In a collision between a heavy ion and an atom, copious electron vacancies are produced in the shells of both collision partners. Often, vacancies are produced in the inner shells which leave the atom or ion in a particular highly excited state. When the de-excitation occurs, the energy is removed through the emission of an x-ray photon or an Auger electron which have energies characteristic of the shells involved.

Two quite different theories have been proposed to explain the production of vacancies in these collisions. One model assumes that the Coulomb field of the projectile interacts directly with the electron of the target atom and thereby promotes it to a higher energy state or into the continuum. The other model, the molecular model, assumes that the collision is slow enough that at each internuclear separation distance the electronic wave functions in the projectile and target atoms can adjust themselves to a molecular configuration appropriate to a diatomic molecule (Kessel and Fastrup, 1973). This re-orientation of the electrons in the molecular states may result in electron excitation.

If the projectile is swift and has a low atomic number such as an alpha particle or a proton, then the excitations are

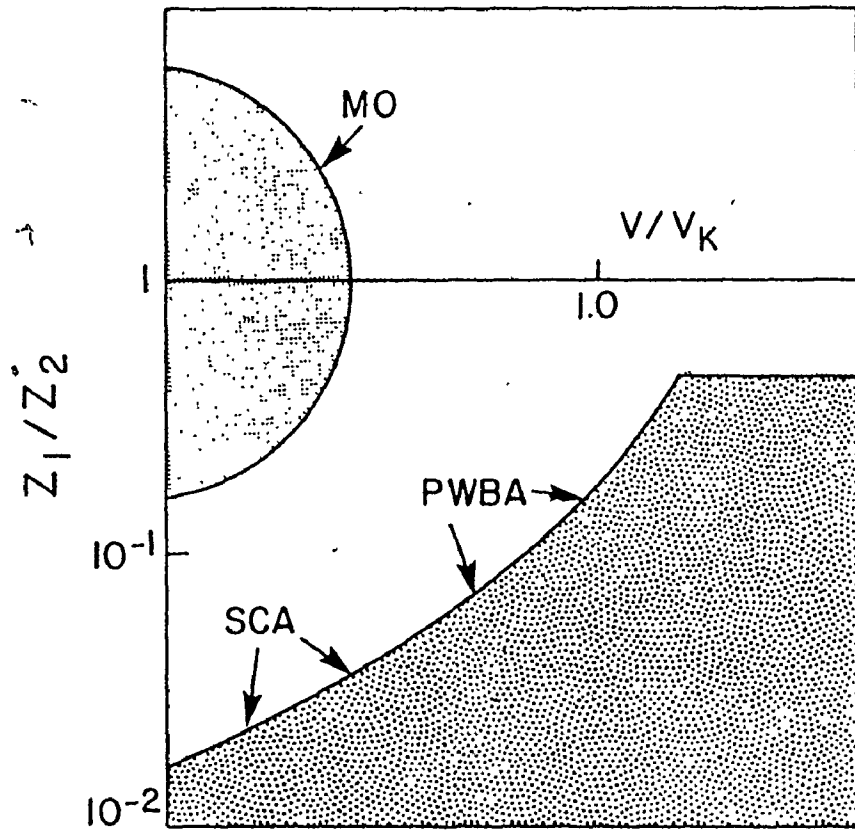
best explained on the basis of a direct Coulomb interaction between the projectile and the ejected electron (e.g. Merzbacher and Lewis, 1958). Classical impulse approximation methods, such as the binary encounter approximation, have been successfully applied to such collisions (Garcia, 1970). Inner-shell excitations become detectable when the relative kinetic energy of the collision partners is much greater than the electronic binding energies of the inner shells involved. The reduced mass of the collision system is much larger than the electron mass so the heavy particles are relatively unaffected by the electron excitations and the plane wave Born approximation becomes applicable (Madison and Merzbacher, 1975). However, if the collision is not swift and also if the masses of the projectile and target are comparable, then these direct Coulomb interpretations give way to the quasimolecular explanation. The regions of applicability of the various models are shown in figure 2-1.

2.2 The Molecular Orbital Model

Inelastic heavy ion-atom collisions are very difficult to describe theoretically. If a direct Coulomb interaction approach is applied, the calculated cross reactions can be orders of magnitude too low in intensity. Approximate methods such as a molecular theory, can be applied and because of the many simplifying assumptions that must be made, the resulting predictions are not definitive. In this section a general outline will be given which will be qualitatively correct but no attempt

Figure 2-1

Regions of validity for various approximation schemes. Z_1 and Z_2 are the atomic numbers of the projectile and target atoms, respectively, v is the projectile velocity while v_k is the K-shell electron velocity. The regions are shown for plane-wave Born approximation (PWBA), semiclassical approximation (SCA) and the quasi-molecular electron promotion model (MO). (cf. Madison and Merzbacher, 1975).



will be made to be quantitative.

The collision process consists of an ion-atom system of two heavy nuclei, separated by a distance $R(t)$, plus the electrons which surround them. Because of the large mass of the nuclei compared with the mass of the electron, it is possible to separate the motions of the nuclei and of the electrons. This is quite a good approximation at low and moderate collision energies in which the relative nuclear velocities are much lower than the orbital velocities of the inner-shell electrons. Thus the inner shell electrons have time to adjust their motions adiabatically to the slowly varying Coulombic fields of the two nuclei. This low velocity situation leads to assumptions of the Born-Oppenheimer approximation (Lichten, 1967). In this approximation the atom-atom system is treated as a quasi-molecule, the electronic states of which correspond to the molecular states of a diatomic molecule. The quasi-molecule varies slowly with time as the internuclear distance first decreases then later increases during the collision.

If the collision takes place at higher energies, then the electronic states of the quasi-molecule are perturbed from the adiabatic levels of the diatomic molecule. The states which are used in the description of this more dynamic process are basis states of the diabatic representation. At these higher velocities the motion of the nuclei may induce inelastic effects such that both inner and outer shell vacancies may be

produced by a molecular promotion mechanism in which electrons of the quasi-molecule are excited to higher lying molecular states or into the continuum. It is through processes of this kind that it is possible for an electron to be in an excited atomic state when the collision partners separate.

Even during a collision, the inner-shell electrons remain tightly bound to one or both of the nuclei and therefore, the electron-electron interactions may be regarded as small compared to the electron's Coulomb interaction with the nuclei. The inner shell electrons may thus be reasonably represented by one-electron molecular orbitals. However, since the electron-electron interaction energies are comparable to the level spacings for outer shell electrons, the one electron picture is much less valid for them.

The de Broglie wavelengths ($\lambda = \frac{h}{p}$) of the nuclei during the collision are small relative to atomic dimensions since the velocities of the nuclei are significantly greater than thermal velocities for which the de Broglie wavelengths are comparable to atomic dimensions. This makes it possible to apply classical mechanics to the scattering of the nuclei off one another which leads to an impact parameter formulation of the nuclear trajectories (Evans, 1955). The electrons are still treated within a quantum mechanical framework.

The model which best explains the production of vacancies for collisions of heavy atoms with low or moderate collision velocities is the molecular one. If it is a good

assumption that the nuclear and electronic motions may be treated independently, the Born-Oppenheimer approximation may be used. The theory treats the coupling between the nuclear and electronic motions as a perturbation of the nucleon-electronic Coulomb interaction. The Born-Oppenheimer approximation gives an adiabatic representation of the electronic states during the low nucleon-velocity collision. The electrons adjust their motions such that molecular states are formed which have definite angular momentum about the slowly rotating and changing internuclear axis. This method has been extended to a collision problem where the internuclear separation varies from infinity to approximately zero. The electronic states then follow adiabatic potential energy curves as the internuclear distance varies. The diagrams which plot the potential energy curves of the electronic states as a function of intermolecular separation are called correlation diagrams.

However, if the collision takes place at higher velocities, the electronic charges will not have time to adjust their motion adiabatically. This means that now the electronic system of the colliding particles will not be able to trace along the adiabatic curves. The diabatic set of basis states is then the most useful representation. As long as it can be determined that the diabatic states will be velocity independent over a broad range of nuclear velocities, they may be a useful representation. For a given collision only a detailed

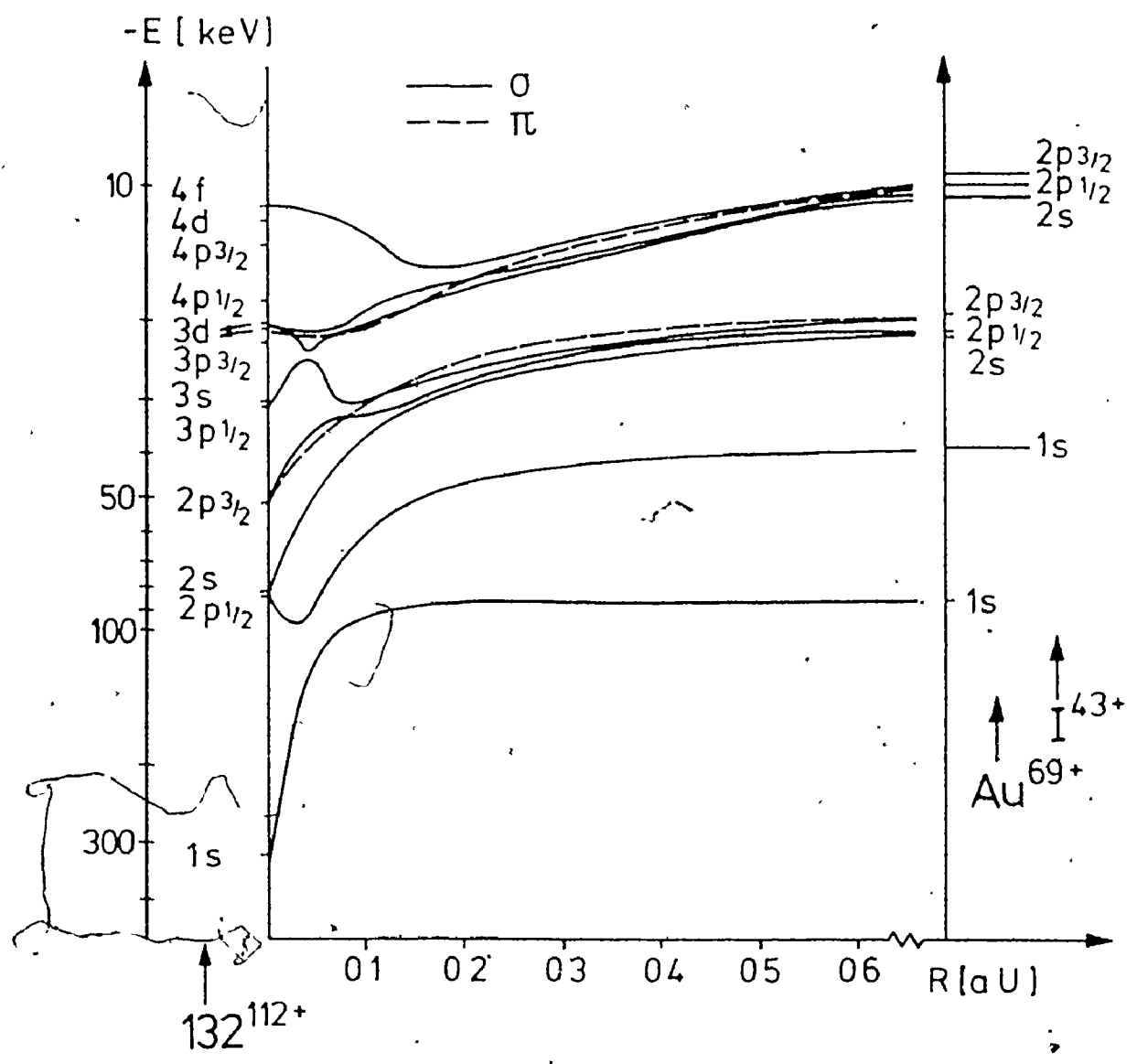
analysis can determine whether adiabatic or diabatic states are good approximations to the states describing the dynamic system.

2.3 Molecular Orbital Correlation

The internuclear separation varies from infinity to approximately zero and back to infinity during a close encounter collision between two atoms. When the separation is very large, the atoms do not interact and are referred to as separated atoms. However, when the two nuclei are close together the electrons surround a nuclear charge the atomic number of which is the sum of the atomic numbers of the collision partners. If the potential energy curves that the electrons follow were known precisely, then it would be possible to predict the electron promotions that would likely result from the collision. Extensive calculations have only been carried out on the simplest diatomic systems (Helfrich and Hartmann, 1970). Little is known about the molecular structure of many-electron diatomic systems which have interatomic separation varying over an extended range. The calculations, which involve several excited molecular states and cover a range of internuclear separations are complicated and difficult in the extreme, Fricke et al. (1975) have tackled the problem of the iodine on gold collision where the calculation has been simplified by considering only the twenty innermost electrons (see figure 2-2).

Figure 2-2

Relativistic many-electron correlation diagram for the system I-Au (20 electron), from Fricke et al., 1975. The energy levels of the separated atoms are shown on the right-hand side and those of united atom on the left hand side.



Fano and Lichten (1965) (also Lichten, 1967) proposed the use of one-electron H_2^+ -like correlation diagrams for the inner shells of more complicated symmetric molecules. Two reasons which justify their choice are, firstly, since the electron-electron interaction is relatively small, the inner-shell electrons may be approximated by a one-electron molecular orbital (MO) as was mentioned earlier, and secondly the adiabatic and diabatic MO's are identical for a one electron system. An example of such a correlation diagram is shown in figure 2-3. Though originally asymmetric collisions, in which the atomic numbers of the two partners are different, were not included, the idea has since been expanded to include these cases (Barat and Lichten, 1972). In order to correlate the atomic orbitals with the MO's at both $R \rightarrow 0$ and $R \rightarrow \infty$, Barat and Lichten have proposed a general rule. They suggest that the diabatic MO's conserve the number of radial nodes of the electronic wave functions which is given by $n-l-1$ (n is the principal quantum number, l is the angular momentum quantum number), as the separation varies from the united atom to the separated atom limits. The assumptions underlying this simple rule are twofold. The inner-shell electrons in a many electron system can be represented by one electron states and the incomplete nuclear screening which causes avoided crossings (von Neumann and Wigner, 1929) for the adiabatic MO's can be ignored for the diabatic MO's. The correlated levels must also have the same value of λ (σ , π , δ , etc), the component of the angular momentum

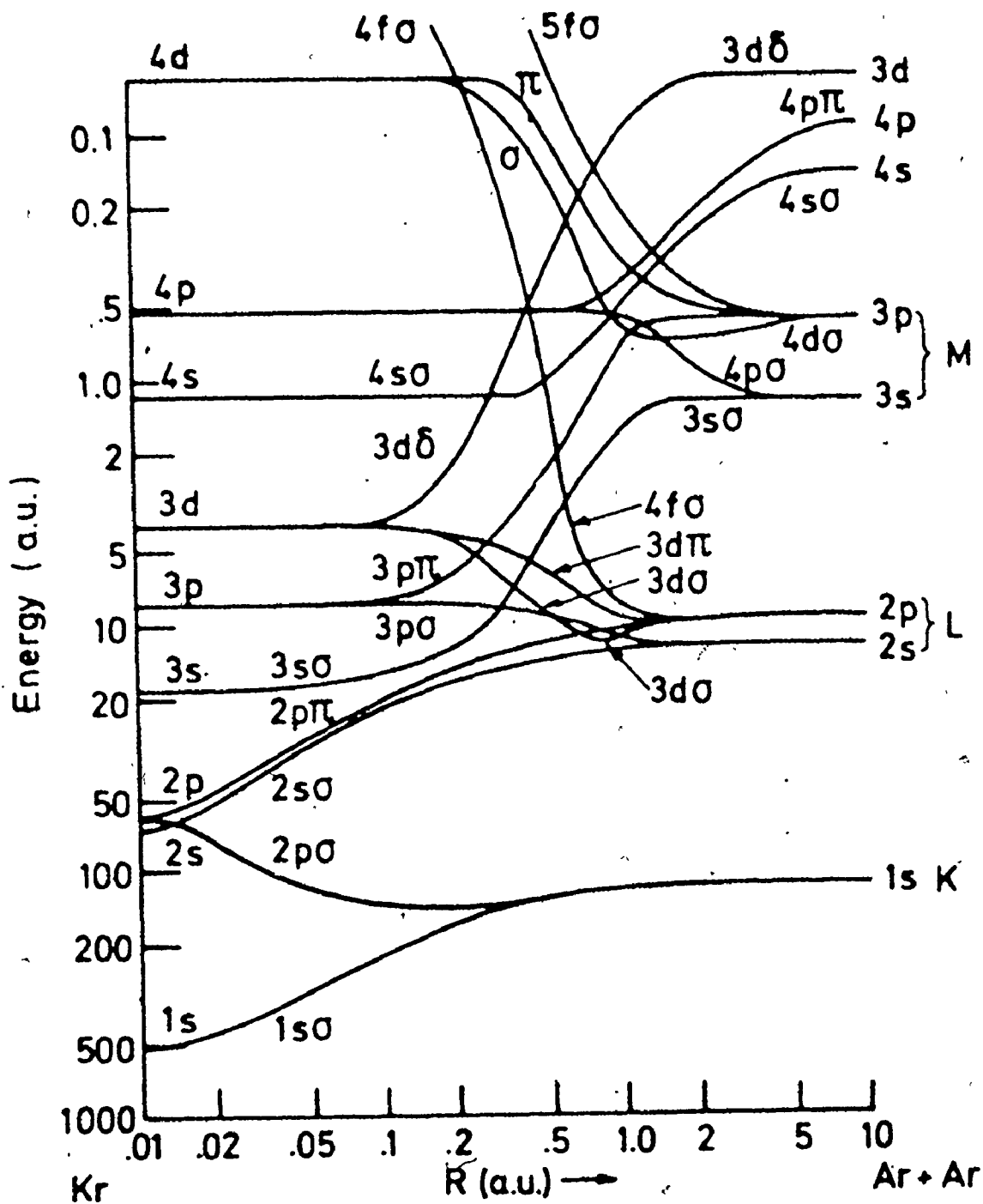


Figure 2-3

Semi-quantitative MO energy level diagram for Ar-Ar molecule as proposed by Fano and Lichten (1965).

vector along the internuclear axis. Simple MO correlation diagrams, based on the above ideas are illustrated in figures 2-4, 2-5 and 2-6 for different cases of projectile and target atomic numbers.

2.4 MO Excitation Mechanisms

The electronic behaviour during a collision is a quantum mechanical problem whereas the motion of the nuclei is described well in terms of classical Coulomb scattering. If a vacancy exists, transitions between MO states may be induced by the motion of the atomic nuclei. There are three categories of perturbing forces which may be responsible for the promotion of electrons and these couplings causing the excitations are designated as potential, radial and rotational (Coriolis) couplings (Kessel and Fastrup, 1973).

The potential coupling is a static coupling and is a result of interactions such as the configuration interaction, the spin-orbit interaction, et cetera. It was stated earlier that if the collision energy is low then the adiabatic representation is a good approximation. The adiabatic basis set will diagonalize the electronic Hamiltonian, H^e , and since there are no off-diagonal elements there can be no coupling. The electronic Hamiltonian is the quantum mechanical operator consisting of the one-electron kinetic energy operator plus the electron-electron and the electron-nucleus interaction potentials (e.g. see Kessel and Fastrup, 1973). However,

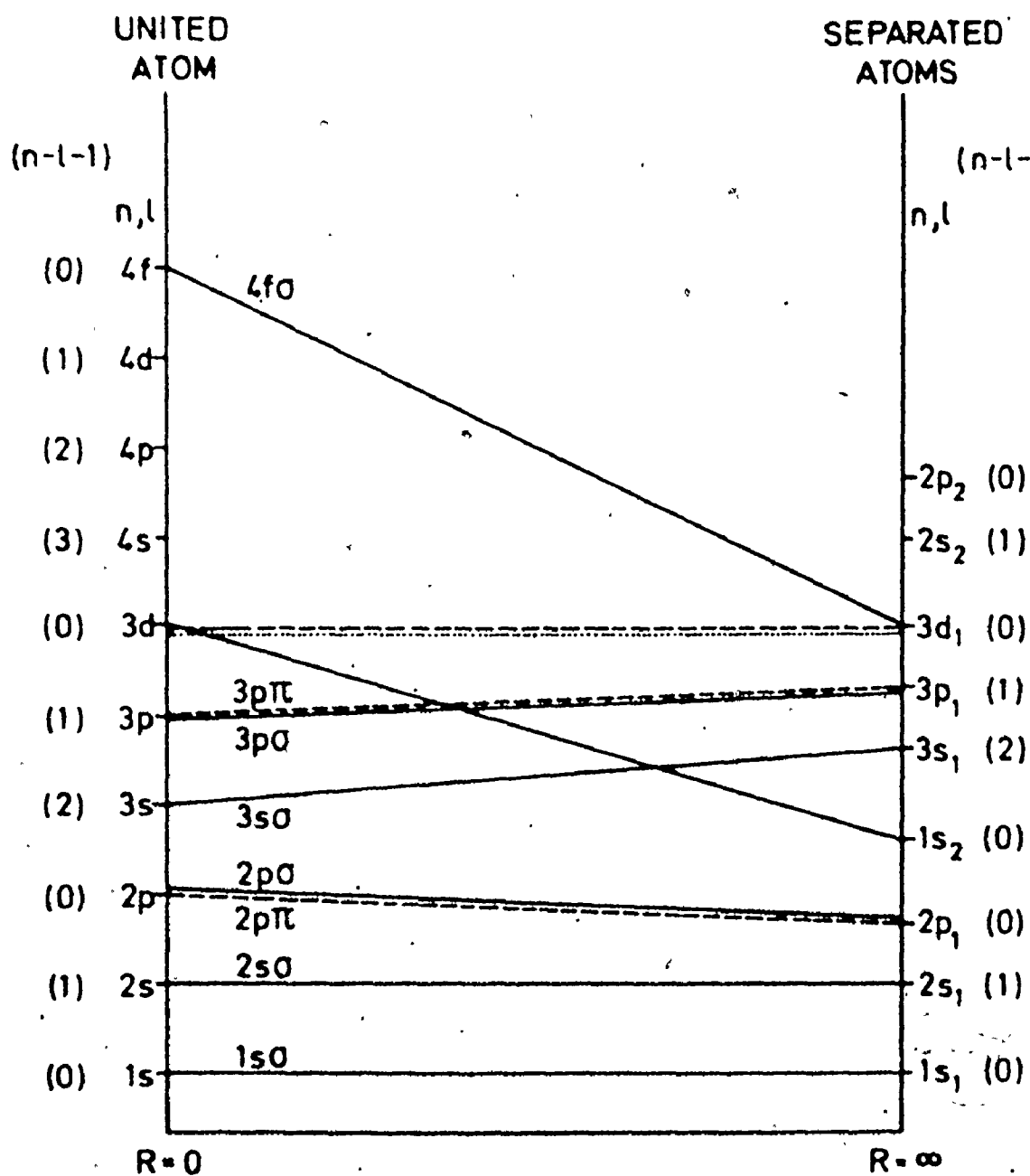


Figure 2-4

Schematic MO-correlation diagram for the case of Z_1 much greater than Z_2 . Electrons are not promoted from the inner shells by an MO mechanism.

Figure 2-5 :

MO correlation diagram for a system for which there exists a near resonance between the 1s level of one atom and the 2p and 2s of the other.

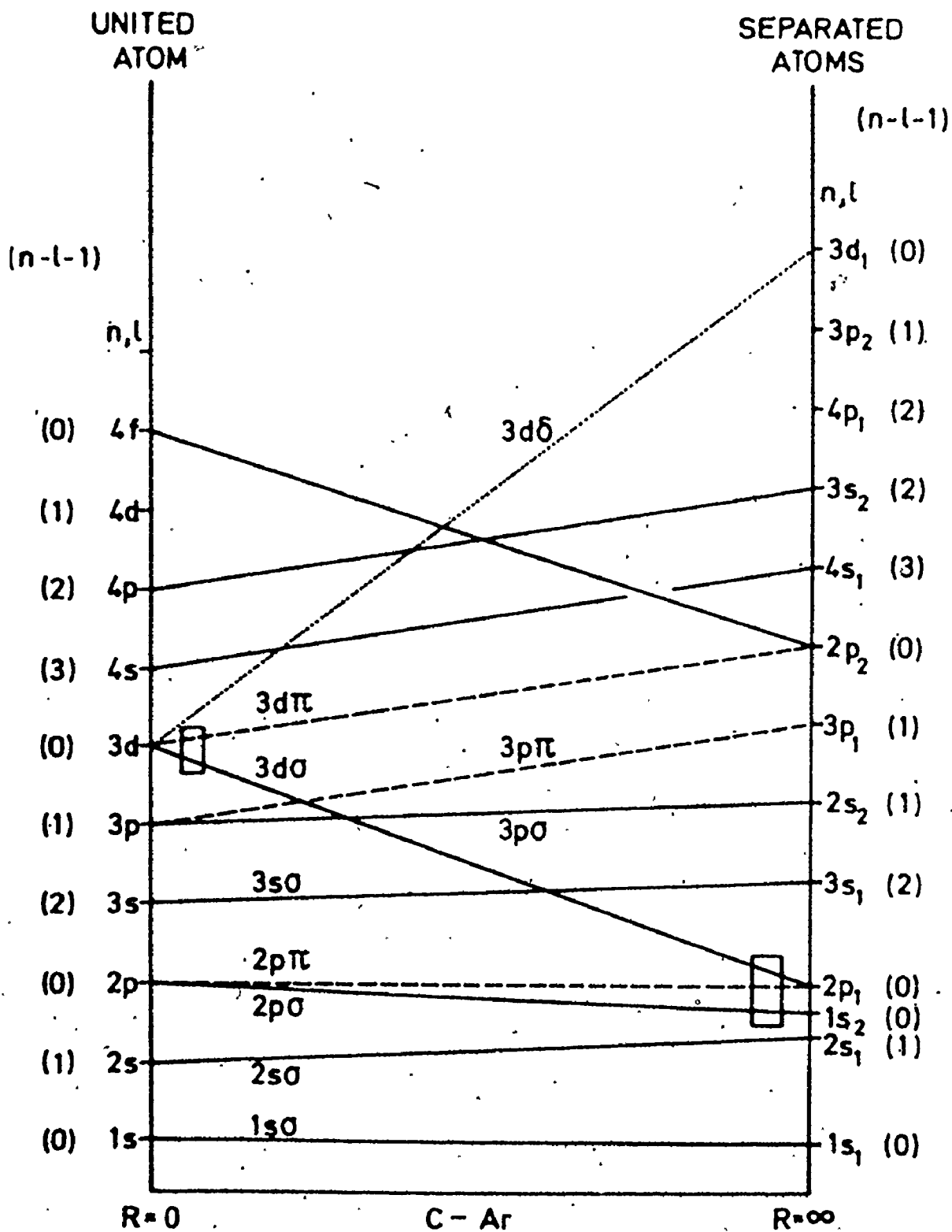
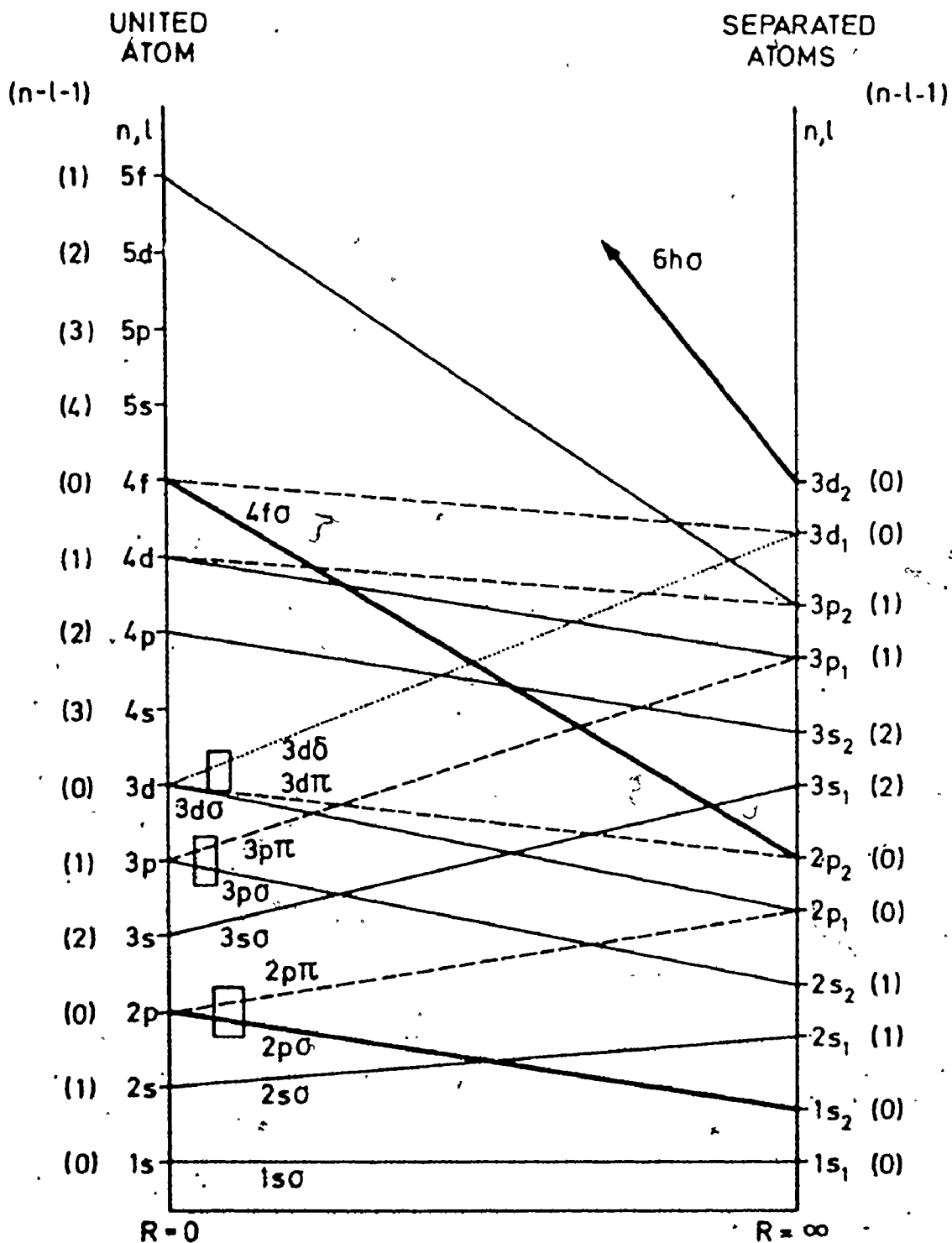


Figure 2-6

MO correlation diagram for the case of Z_1 slightly larger than Z_2 . The σ MO's $2p\sigma$, $4f\sigma$ and $6h\sigma$ are responsible for promotion of K, $L_{2,3}$ and $M_{4,5}$ electrons, respectively. The rectangles show where rotational coupling interactions between two MO's may be expected.



at higher energies it is more appropriate to use the diabatic states which will not normally diagonalize the potential energy matrix $\langle \psi_m^e | H^e | \psi_k^e \rangle$ and hence the off-diagonal elements show that transitions between diabatic states may occur (ψ_m and ψ_k represent the electronic wavefunctions of the states m and k).

The radial and rotational couplings are both dynamic and thus, unlike the potential coupling, depend on the velocity of the collision. Consider first the radial coupling term in the time-dependent Schrödinger equation of the electronic motion,

$$v_R \langle \psi_m^e | \frac{\partial}{\partial R} | \psi_k^e \rangle$$

where R is the internuclear separation. The perturbing force causing the coupling is seen to be dependent upon the radial velocity, v_R , and for larger values of the collision velocity the radial coupling may become quite appreciable. The non-diagonal elements will be non-zero only if the two states k and m have the same symmetry, that is the same projection of angular momentum (e.g. two σ states), spin and in the case of homonuclear systems, parity (Levine et al. 1969).

The rotational coupling depends on the velocity and the impact parameter of the collision, and inversely as the square of the separation of the two colliding partners. The mutual rotation of the two nuclei about one another causes the interaction between electronic states. For a given trajectory of the

incident ion, the rotational coupling term is given by

$$\frac{v_0 b}{R^2} \langle \psi_m^e | L_y | \psi_h^e \rangle$$

where v_0 is the incident ion velocity and b is the impact parameter. The rotational operator L_y couples only those states for which the angular momentum differs by one unit and those states that have the same spin, and if it is a homonuclear collision, parity (Russek, 1971). The operator has the property that it will couple only the x and z components of the m and k states together. Since the rotational interaction couples only those states with different angular momentum projections, the rotational coupling does not couple the same states that the radial coupling does. The rotational coupling, depending on both the velocity of the collision and on the impact parameters, results in characteristic excitation functions (Russek, 1971) which should be distinguishable from excitation functions due to potential and radial couplings.

Approximate calculations of inner shell excitations for actual collisions are so extremely complex that few have been computed. It is this difficulty which makes the simple diabatic MO correlation diagrams so valuable. The value of the diagrams may be shown by using figure 2-6 to illustrate how inner L and K vacancies may be produced.

For the case where the atomic numbers of the projectile and target atoms are comparable, it is observed experimentally that once the two atoms approach each other within a

critical distance there is a strong resonance for the production of L-shell vacancies in the lighter of the two collision partners (Fastrup et al., 1971). This would indicate that a MO is rising steeply through a whole series of crossings with other MO's into which any one of these possibly vacant MO's, an electron could be promoted. The diabatic $4f\sigma$ MO meets these requirements as vacancies may then be left in a $2p_2$ state (the subscript 2 refers to the lower z. partner, subscript 1 the high z partner) of the separated atom.

Now consider, for the production of K x-rays, that the $2p_1$ state has a vacancy when the two colliding atoms are at a large separation. If this is so, then as the separation approaches zero, a rotational coupling could then promote an electron from the $2p\sigma$ MO to the vacancy in the $2p\pi$ MO. Thus upon separation of the two atoms a K-vacancy may be produced in the lighter atom.

The application of the MO model to inner shell excitations is subject to two major conditions. The conditions are that the atomic numbers of the colliding atoms are not very different and also that the impact velocity is smaller than the orbital velocities of the inner shell electrons. If these criteria are not met then the MO model may not be applied and some other model, such as a direct Coulomb approach should be tried. But in those situations in which the conditions are fulfilled, then the success of this model is well established (Kessel and Fastrup, 1973).

CHAPTER 3

EXPERIMENTAL TECHNIQUES

3.1 Introduction

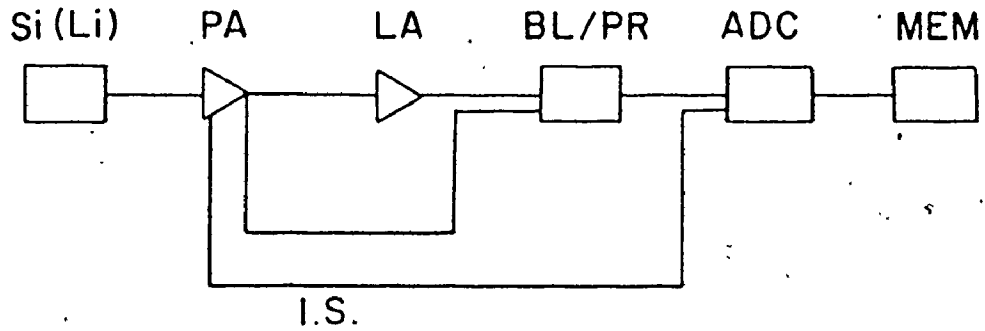
This thesis deals with a study of x-ray emission when various elemental targets are bombarded by heavy ion beams with energies in the region of 0.6-0.8 MeV/amu. One aspect of this study deals with the x-ray continua that results. These studies have been carried out using a "singles" method in which only one solid-state detector is used in the acquisition of data. The other aspect considered is the production of double K-shell vacancies. These data were collected using a coincidence technique using two solid-state detectors which may have energy signals in coincidence and so may indicate a double K x-ray event.

3.2 X-ray Continua Techniques

The x-ray data collected in the study of the continua were obtained from the bombardment of a thin gold foil by a number of different projectiles from the FN tandem accelerator. These beams had energies of 0.76 MeV/amu. The self-supporting gold target ($90 \mu\text{g}/\text{cm}^2$) was mounted at 45° to the beam direction and the radiation produced was detected with a 5mm thick, Si(Li) detector with full width half maximum (FWHM) resolution at 6.4 keV of 185 eV. The detector was rotated about the

target at angles from 30° to 150° with respect to the beam direction. To attenuate the very intense characteristic x-rays of the projectile and target, a 0.87 mm thick aluminum sheet was used as an absorber. The target chamber was made of perspex and had a wall thickness of 1/4 inch. An experimental difficulty that requires consideration is electronic pulse pile-up in which pulses occur within the linear amplifier resolving time. A pulse pile-up rejection system was used during the acquisition of data. A schematic diagram, figure 3-1, shows the electronics used in these experiments.

There are two types of pile-up which cause problems in the energy region of the continua. The first type is random coincidences of two unrelated characteristic x-rays which if summed together have an energy in the region of the continuum and which may become a significant background contribution. A pile-up rejector is used to determine whether an input pulse is contaminated by a second pulse due to piling up or whether it follows a previous pulse in less time than that selected by a deadtime control. A third restriction is that the detector signal must not have a risetime greater than normal. If any of these events occur, that pulse is rejected. As a preventative measure to minimize this pile-up the count rate of the detector is kept at 500 counts per second, so that random coincident pile-up was not detectable.



Si(Li) - detector

P.A. - preamplifier

LA - linear amplifier

BL/PR - baseline restorer, pileup rejector

ADC - analog to digital converter

MEM - memory of PDP-9

I.S. - inhibit signal from pulsed optical
feedback.

Figure 3-1

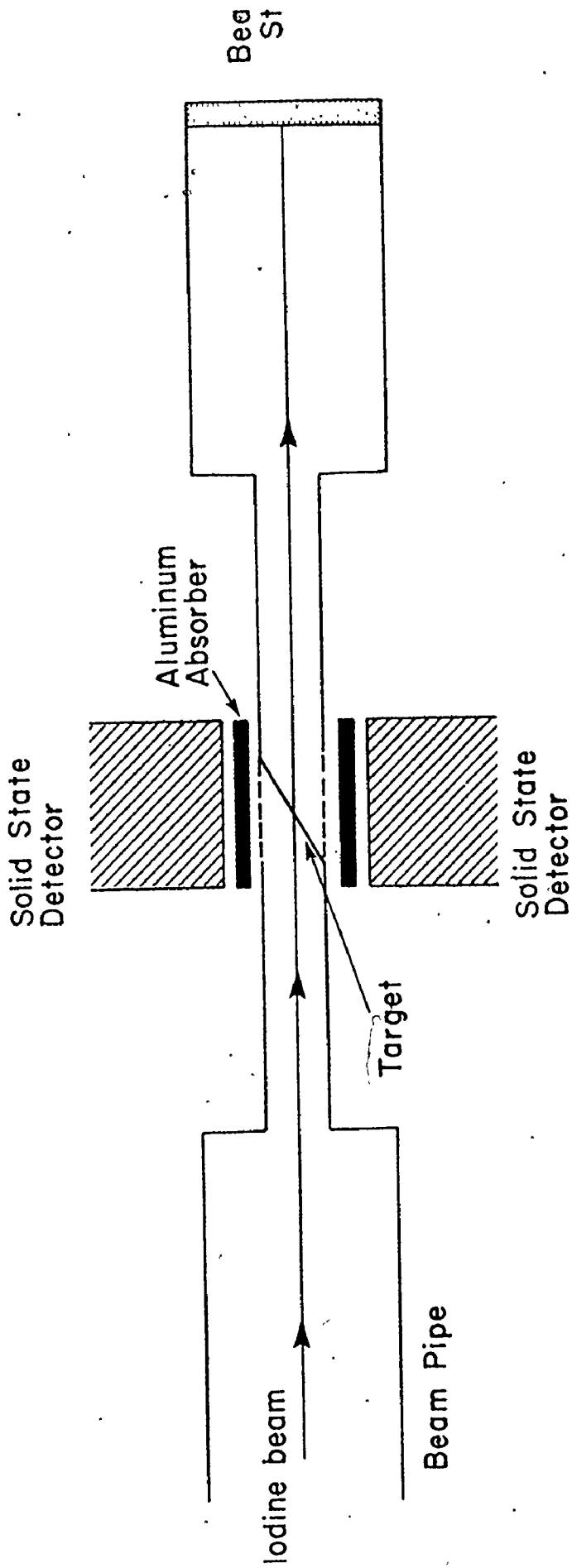
Schematic diagram of the electronics of singles
experiment.

The other type of pile-up is due to true coincidences in which two x-rays (or more) which have been produced by the same beam particle, impinge simultaneously on the detector. This kind of pile-up is minimized by decreasing the solid angle of detection since the probability of detecting the simultaneous events depends on the square of the solid angle.

3.3 Double K X-ray Techniques

A beam of 80 MeV $^{127}\text{I}^{10+}$ ions from the FN tandem accelerator was directed and focussed through a pair of 3 mm apertures 41 cm apart onto a target positioned inside a target chamber of width 1.2 cm (see figure 3-2). Thin plastic windows on either side of the target were 1.5 cm in height, 2.0 cm in length and 0.13 mm in thickness. In order to maximize coincidence efficiency, the detectors were positioned as close to the windows as was feasible and had either a 0.43 or 0.87 mm aluminium absorber to attenuate the intense L and M x-rays. The targets were oriented at an angle of 30° with respect to the beam direction. The targets were $70 \pm 30 \mu\text{g}/\text{cm}^2$ thick and were placed on a backing of carbon of thickness $30 \mu\text{g}/\text{cm}^2$ or $50 \mu\text{g}/\text{cm}^2$.

This experiment was designed to observe the decay of an atomic state which has two vacancies in the K shell of the atom. If the state decays by emitting two K x-rays, then by observing x-rays in coincidence the double vacancy state may be detected. The x-rays were detected by two solid state detectors (Si(Li); Ge(Li) or Ge) placed opposite each other



Schematic Diagram
Of Chamber & Detector

Figure 3-2

Schematic diagram of experimental arrangement for the double K-vacancy coincidence experiments. The dashed lines represent thin plastic windows.

Figure 3-3

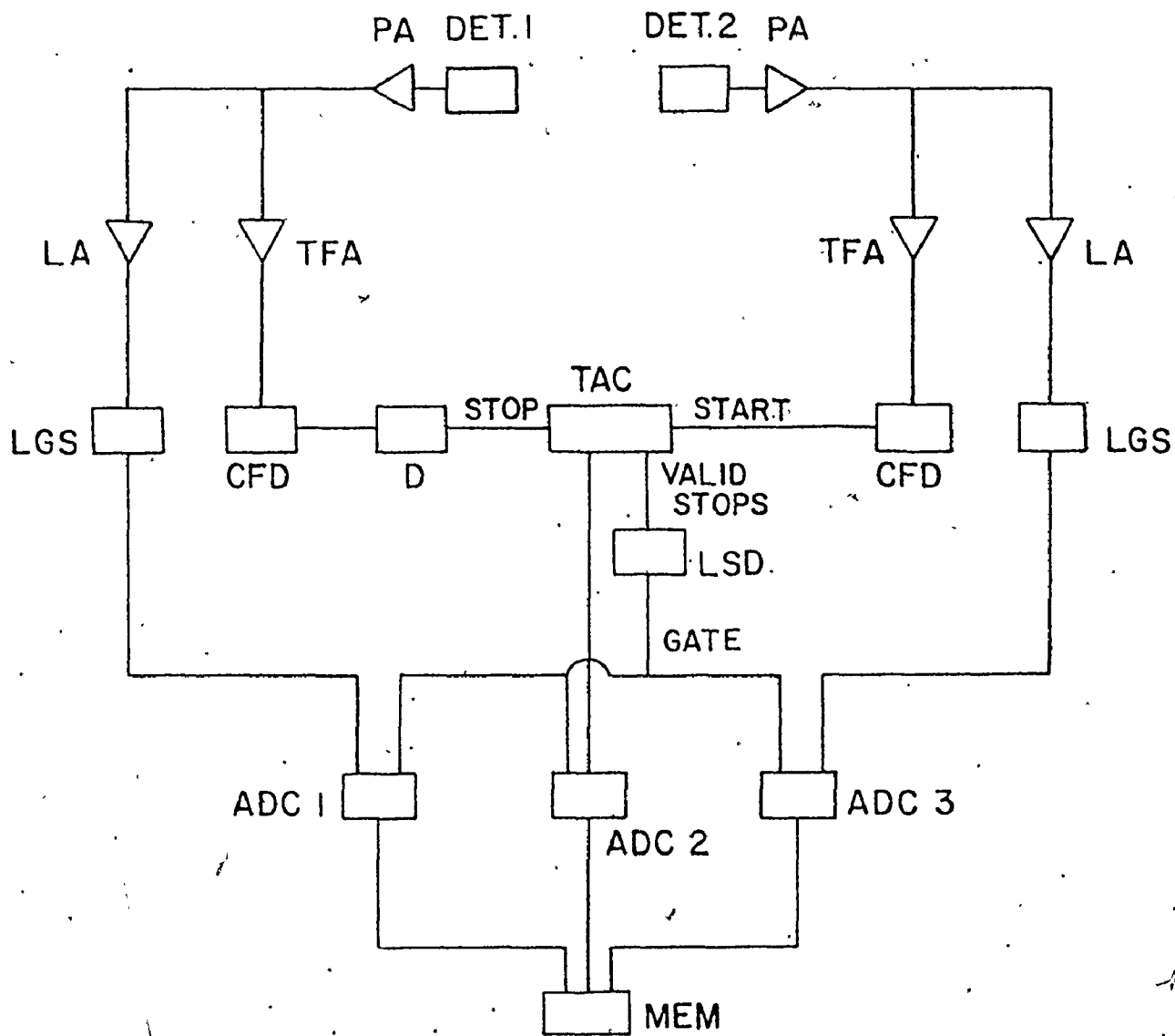
Photograph of x-ray coincidence chamber with target holder in place. The beam stop section is not present.



and at 90° to the beam direction. The electronic arrangement is very similar to the electronics used in nuclear physics γ - γ coincidence experiments (e.g. Hamilton, 1975) and the particular arrangement used in these experimental studies is illustrated in figure 3-4. The electronics was set up such that the energies of the two x-rays and the time difference between them were obtained. These three bits of information were then stored on magnetic tape for later analysis to make a distinction of the intensity of coincidence events which are due to true coincidences from the intensity which is due to random coincidences.

3.4 Timing and Background Considerations

Even though the coincidence electronics used in the experiments are well known, an elaboration of the timing problems encountered should be noted. In order to minimize the chance coincidences during an experiment great care must be taken to reduce the timing uncertainty brought about by the intrinsic time jitter of the detector signal and the timing walk due to amplitude and rise time variations. To accomplish the reduction in timing jitter the electronics were placed physically close to the detectors so that long cables which degrade the signal were not used. This has the additional advantage in that it also results in an improvement in the resolution of the energy signals. Amplitude and rise time compensation is achieved by triggering on the fast preamplifier signal at a constant fraction of the pulse height.



PA - preamplifier
 LA - linear amplifier
 TFA - timing filter amplifier
 LGS - linear gate stretcher
 CFD - constant fraction discriminator
 D - delay
 TAC - time-to-amplitude converter
 LSD - logic shaper and delay
 ADC - analog to digital converter
 MEM - PDP-9 memory

Figure 3-4

Schematic diagram of electronics of double K-vacancy experiments.

In this technique the input pulse is fed through two paths. Along one path, the input pulse is shaped and attenuated to a fraction of its original height. Along the other, the pulse is shaped, inverted and delayed by an interval T_D . Both signals are then added together to form a zero-crossing signal. A zero-crossing discriminator triggers at the zero-crossover point. Since the time of zero-crossing is essentially independent of pulse height, the timing walk of the system is minimized. A timing signal from one detector is fed into the start side of a time-to-amplitude converter while a timing signal from the other detector is fed into the stop side, so that the relative time difference between the signals is established.

An interesting problem arose when the timing electronics were initially set up according to the standard procedures for Ge(Li) detectors. It was discovered that the timing resolution was extremely poor which was due in part to the poor leading edge characteristics of the x-ray pulses. The reason for this is based on the low energy of the x-ray photons relative to the γ -ray photons that are normally used in timing, which because of their greater energy have very sharp leading edges. A significant improvement in the coincidence timing was achieved by adjusting the pulse shaping and delay factors according to the particular detector involved. In general larger integration times were required for these low energy x-ray pulses and also longer delays for

the inverted signal in the constant fraction timing.

The cross section for the production of double vacancies is very small compared to the single vacancy cross sections, so it is important to treat carefully the chance background in the experiments. A typical TAC spectrum is shown in figure 3-5, where a true prompt coincidence peak is superimposed on a continuous background of chance coincidences. The peak-to-background ratio will depend on the resolving time of the electronic circuitry and the x-ray intensity, N . If the product of the detector efficiency and solid angle is represented by $(\epsilon\omega)_i$, where i signifies the detector, then the counting rates are given by

$$N_1 = N(\epsilon\omega)_1 \quad N_2 = N(\epsilon\omega)_2$$

The true coincidence rate is given by

$$T = FN(\epsilon\omega)_1(\epsilon\omega)_2 \epsilon_e$$

where F is the proportion of the x-ray intensity giving coincidence events and ϵ_e is the electronic efficiency. The chance rate for a spectrum with a prompt peak of width τ is

$$C = N^2(\epsilon\omega)_1(\epsilon\omega)_2\tau\epsilon_e$$

The ratio of true-to-chance coincidences will therefore be given by

$$T/C = \frac{F}{N\tau}$$

Time Spectrum of Indium Experiment.

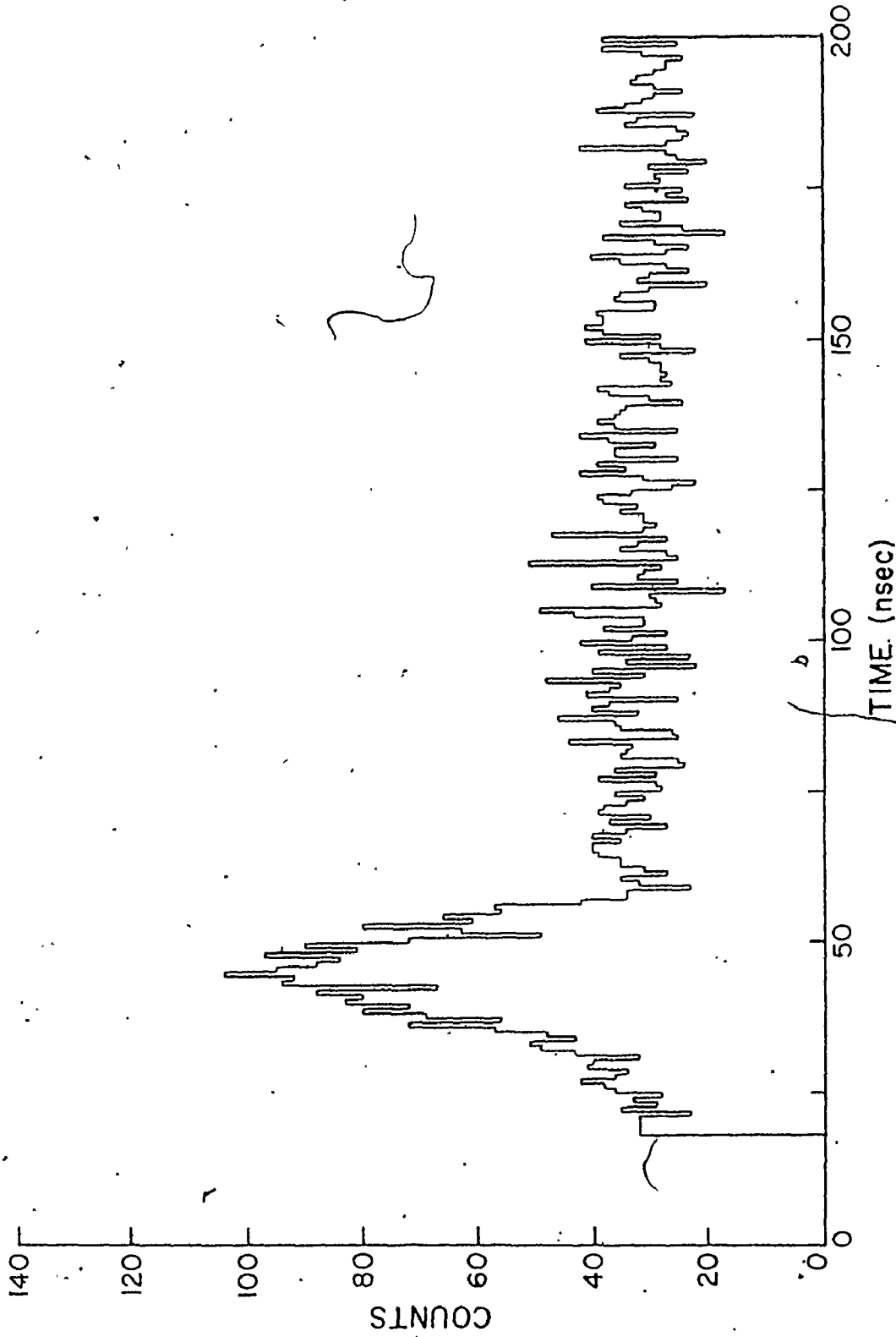


Figure 3-5

The time spectrum from the TAC for the iodone on indium experiment.

Assuming that the timing resolution τ has been minimized, the true-to-chance ratio is optimized by reducing N , that is, reducing the beam current on target. Even though N is reduced the true count rate is kept at an acceptable rate by placing the detectors as close to the target as possible (maximizing the solid angle). Typically the count rates in the detectors were 500 to 1000 counts per second while the true coincident count rate was of the order of one count per minute. The true-to-chance ratios were approximately one to one in the prompt peak.

3.5 The X-ray Detectors

During the course of these experiments three different solid state detectors were used, a lithium drifted silicon detector (Si(Li)) of 78 mm^2 sensitive area, a lithium drifted germanium detector (Ge(Li)) of 750 mm^2 sensitive area and an intrinsic germanium detector of 1450 mm^2 sensitive area. The FWHM resolution obtained for the 27.4 keV Te K α combined line (see appendix for notation) is 545 eV, 795 eV and 865 eV for the Si(Li), Ge(Li), and Ge detectors, respectively. The significance of these numbers is that for the first experiments it was necessary to have good resolution in order to determine which x-rays were in coincidence with which other x-rays. The resolution was obtained at the cost of counting rate since the solid angle of the Si(Li) detector is relatively smaller. However, in later experiments in order to gain good statistics the higher counting rate was obtained with the Ge and Ge(Li)

combination. In figure 3-6 the absolute efficiencies of the respective detectors as measured with a calibrated source with a .43 mm aluminium absorber and in the actual geometry of the experiments is shown as a function of photon energy.

3.6 The Iodine 125 Source

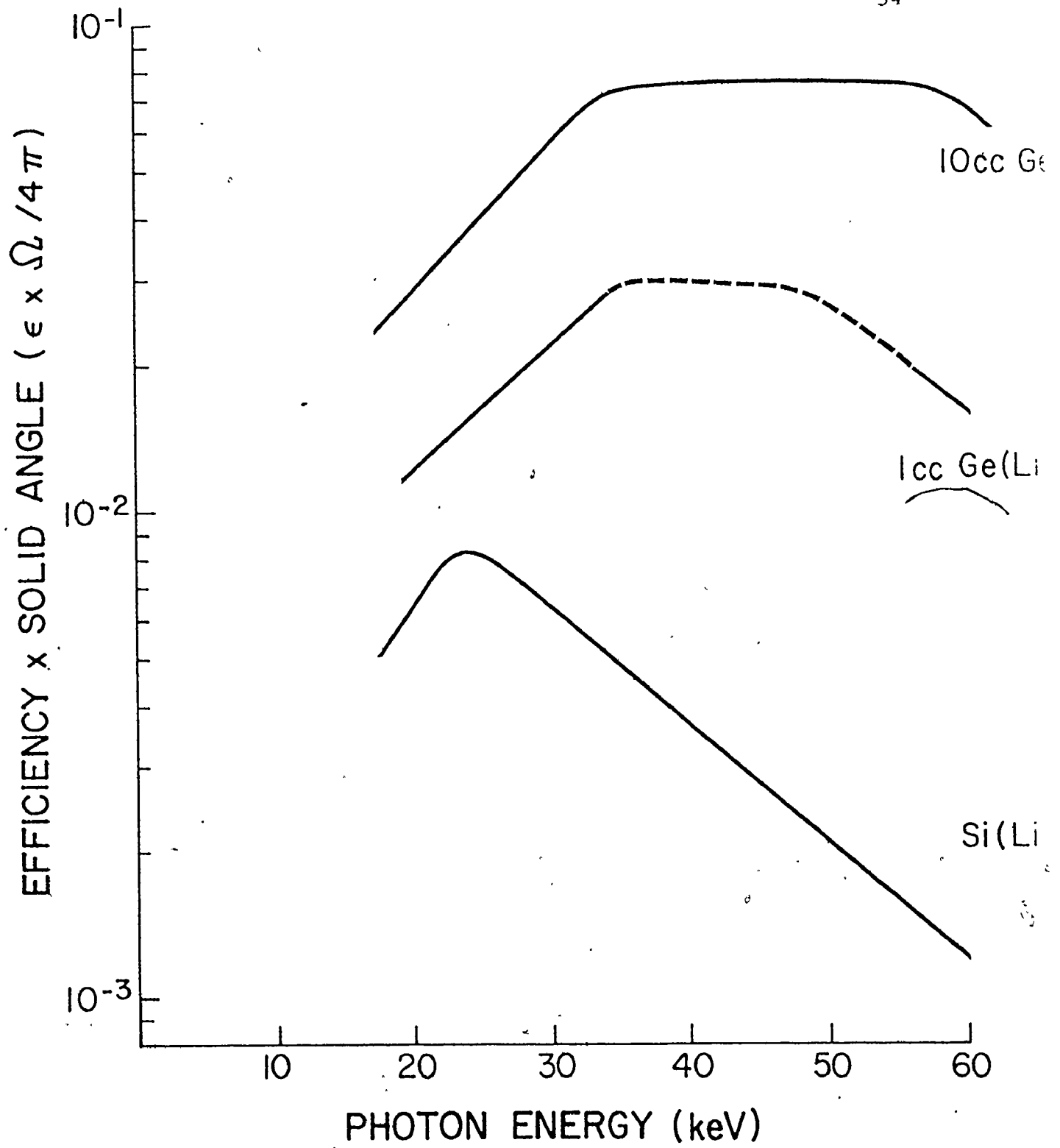
In order to set up the coincidence electronics it was necessary to simulate as closely as possible the experimental electronic situation. Normally in a nuclear γ - γ coincidence experiment standard sources are available which emit relatively high energy photons that are in coincidence. For the purposes of the x-ray experiments none of the standard coincidence sources were quite appropriate. What is required for this type of experiment is a source which emits coincidence photons in the x-ray region of about 30 keV. Another criterion is that the source have a reasonably long lifetime such that the source sample is convenient to use. The ^{125}I isotope which has a half-life of 60 days was found to be ideal. This isotope decays to ^{125}Te through the process of electron capture in which for 80% of the decays (R. L. Auble, 1972), the electron captured is a K-shell electron. Thus a K x-ray of tellurium is produced. The nuclear level populated by the electron capture is the low lying first excited 35.46 keV state of ^{125}Te which is strongly internally converted, the K conversion coefficient (the ratio of K conversion electrons to gamma rays emitted in the decay of the nuclear state) being 11.8. Thus

Figure 3-6

The absolute efficiencies for the three detectors used in the coincidence experiments. The curves represent the product of the geometrical ($\Omega/4\pi$) and the full energy absorption efficiency (ϵ) of each detector. The uncertainty associated with these curves is 40%.

Absolute Efficiency Curves

34



another K hole may be produced which may result in an x-ray. Since the half-life of the excited 35.48 keV state is 1.49 nanoseconds, the two x-rays are coincident within the 30 ns resolving time of the experiment. A 35.48 keV gamma ray may also be in coincidence with the original x-ray. The spectrum of photons emitted by the source is shown in figure 3-7.

3.7 Coincidence Analysis Considerations

The coincidence data were collected on magnetic tape with each coincident event stored in a three word digital form to represent an energy from one detector, an energy from the other detector and the time difference between the detection of these two x-rays. The energy spectra of each of the two detectors and the time spectrum were stored in three regions of the PDP-9 computer memory during the course of an experiment in order that the spectra being collected could be monitored. The three spectra are called projections. If the coincidence events are thought of in terms of a 3-dimensional matrix with two of the axes being the energy axes for the two detectors and the third axis being a time axis for the time differences, then the sum of all coincidences can be projected onto any one of the axes. Illustrations of the three projections are shown in figures 3-5, 3-8 and 3-9.

Since the total number of coincidence events is relatively small (of the order of ten thousand) and the true to chance ratio is about one to one it is very important to treat the chance subtraction very carefully. In the time spectrum the

Figure 3-7

The spectrum of x-rays emitted by an iodine 125 source
as detected by the Si(Li) counter.

Spectrum of Iodine 125 Source

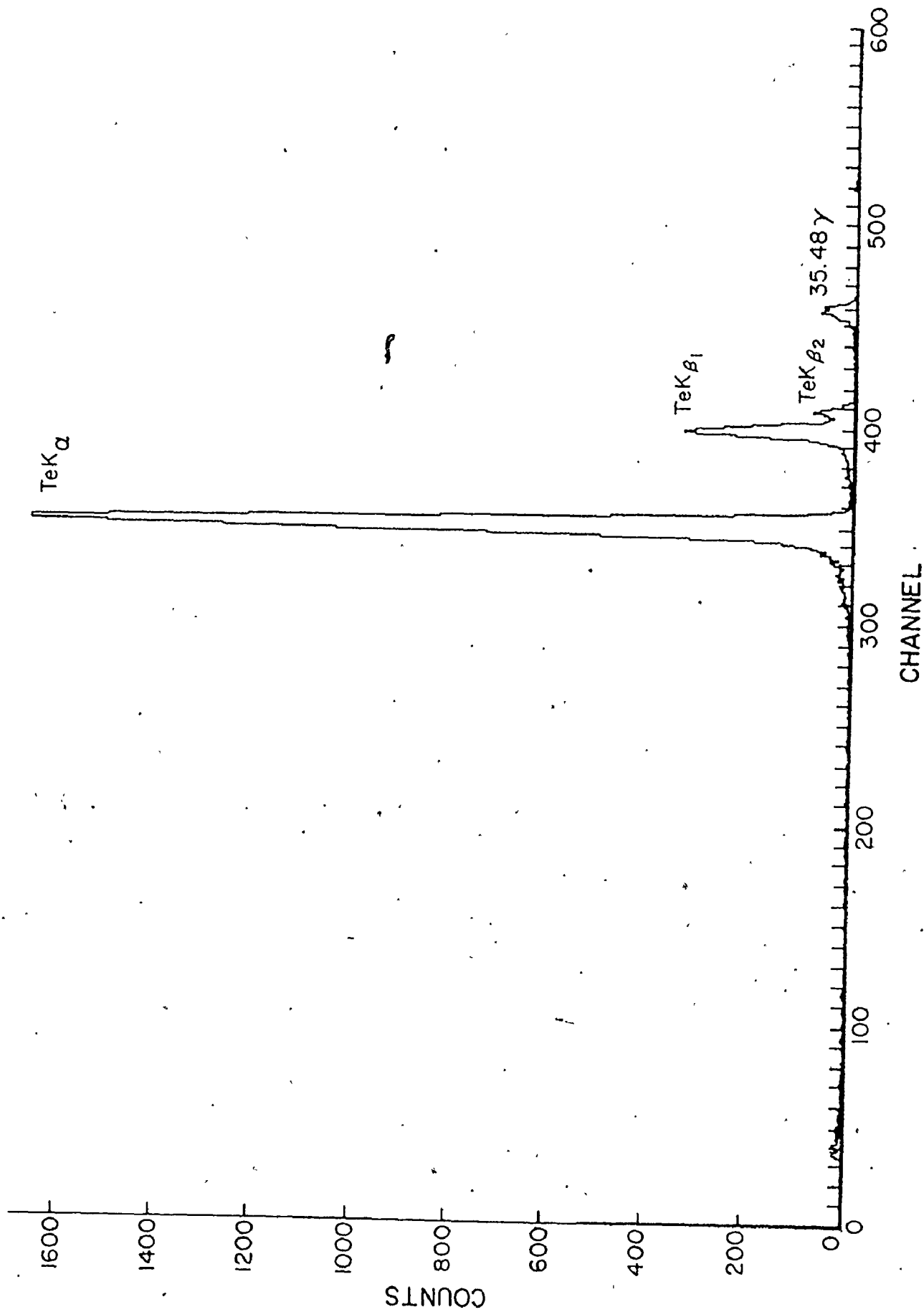


Figure 3-8

The spectrum of all K x-rays as collected by the
Si(Li) detector in the iodine on indium experiment.

Si(Li) Projection of Indium Experiment

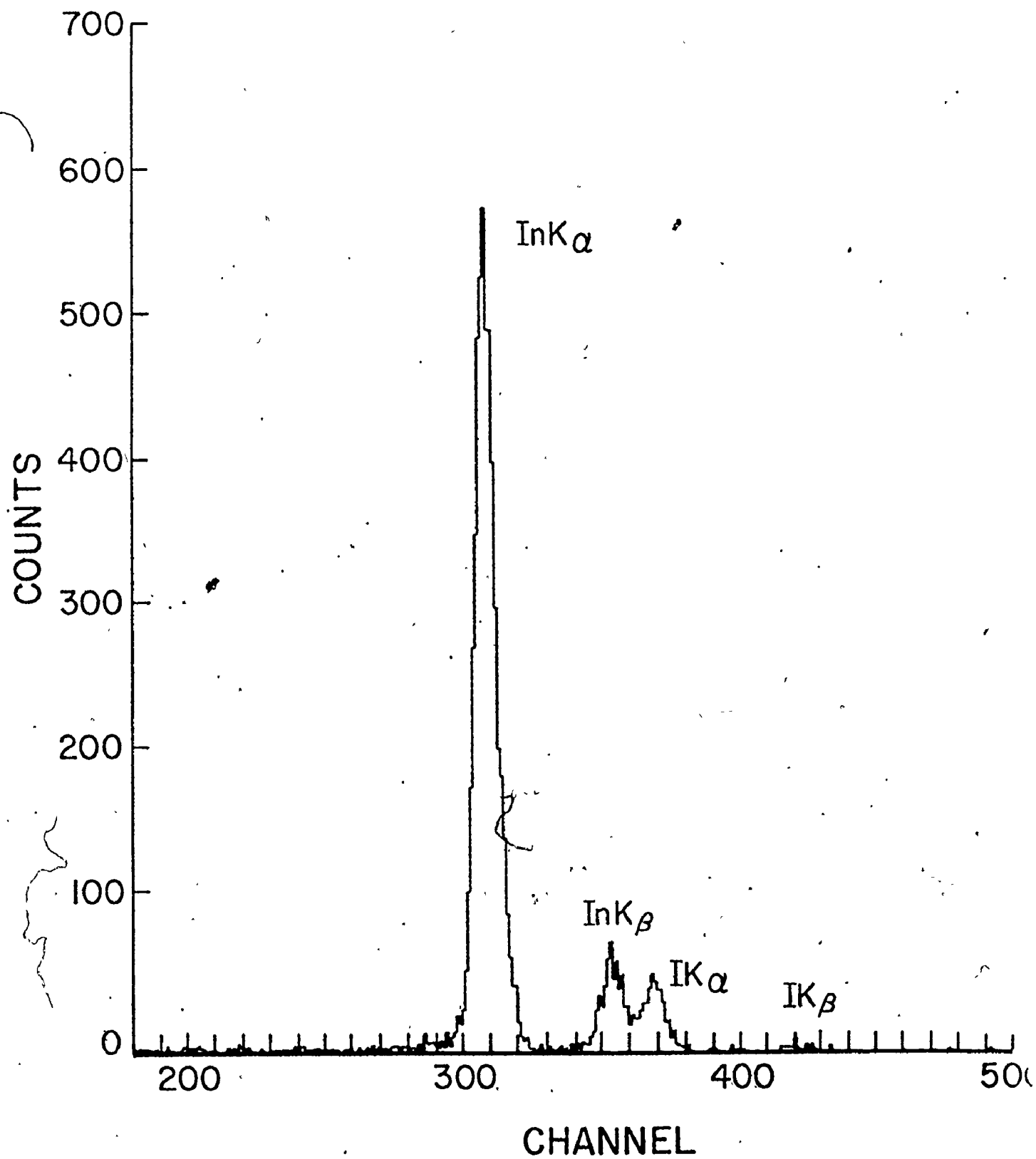
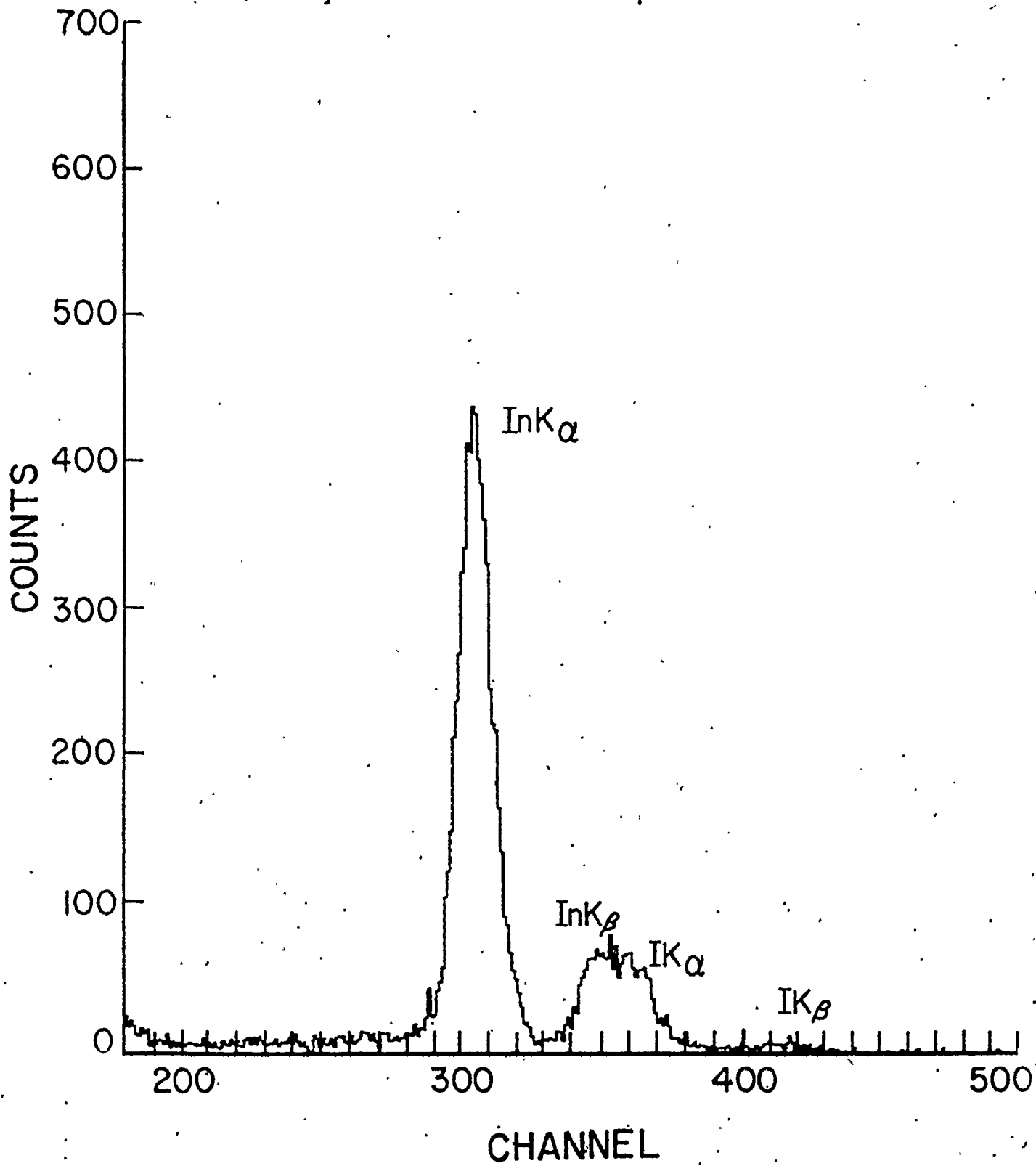




Figure 3-9

The spectrum of all K x-rays as collected by the Ge(Li) detector in the iodine on indium experiment.

Ge(Li) Projection of Indium Experiment



channels over the prompt peak were selected as a coincidence window. The x-rays associated with this region of the time spectrum consist of the true coincidence events, plus the underlying chance event background. A similar gate (or window) was set for the channels extending from just greater than the prompt peak to near the end of the time spectrum. The width of this chance window was typically about five times the width of the prompt window. The range of the total time spectrum for these experiments was either 200 or 500 nanoseconds.

Gates were set on the x-ray peaks of one of the detector's energy spectrum. The x-rays which are in coincidence with the gated x-ray peaks are sorted and separated according to whether the time separating them falls within the prompt gate or within the chance gate. The result of this sorting procedure is that two matrices are formed, one corresponding to the prompt peak events, T_{ij} , and the other corresponding to the chance events, C_{ij} . One axis of the matrices (denoted by index i) is the energy spectrum of the non-gated detector while the other axis (denoted by index, j) consists of the peak gates in sequential energy order.

In order to determine the chance background in a given energy window, j , for a specific energy, i , the probability of having an energy within the gate is multiplied by the probability of having that energy times the total number of chance events.

$$\bar{C}_{ij} = \frac{\sum_i C_{ij}}{\sum_{ij} C_{ij}} \times \frac{\sum_j C_{ij}}{\sum_{ij} C_{ij}} \times \sum_{ij} C_{ij}$$

$$= \frac{\sum_i C_{ij} \sum_j C_{ij}}{\sum_{ij} C_{ij}}$$

where the C_{ij} 's represent the chance event matrix elements. The chance subtracted true prompt coincidence matrix elements are thus given by

$$T'_{ij} = T_{ij} - \frac{\tau_T}{\tau_C} \bar{C}_{ij}$$

where T_{ij} represent the prompt matrix elements and τ_T and τ_C are the time widths of the prompt and chance time gates, respectively. This procedure minimizes the effect of the background subtraction on the statistical fluctuation of the true prompt event spectrum.

CHAPTER 4

X-RAY CONTINUA EXPERIMENTS

A number of authors have reported the observation of radiation continua from collisions of heavy ions which have been interpreted as molecular orbital K x-ray radiation (J. R. MacDonald et al. 1973; W. E. Meyerhof et al., 1973; Davis and Greenberg, 1974). The production of L and M x-rays from combined systems has also been reported (F. W. Saris et al. 1972; P. H. Mokler et al., 1972). In an attempt to observe the MO L x-rays of a very heavy system, a gold target was bombarded with 60 MeV ^{79}Br ions. Radiation continua were produced in this experiment but it will be shown that this radiation cannot come predominantly from molecular orbital shells.

The MO x-ray radiation is the radiative decay of vacancies occupying transient molecular orbitals during heavy ion-atom collisions. If an x-ray were to be emitted where the nuclei were in close proximity, the radiation would have a maximum energy characteristic of the combined atomic numbers of the two nuclei. During the violent collision process the combined-atom lines are shifted up in energy and the spectral peaks broadened. Thus a significant amount of collision broadening (Macek and Briggs, 1974) occurs which increases the energy of the end point of the continua from the united

atom limit. The slopes and maximum energies of the continua should be characteristic of the collision particles involved.

Another important consideration in the observation of MO x-rays is the angular distribution of the radiation. According to Müller and Greiner (1974) the radiation consists of two components, a spontaneous part and an induced part. The spontaneous radiation is isotropic just as the characteristic radiation is isotropic. However, the induced radiation which is brought about by the rotation of the atoms about the centre of mass has a radiation pattern peaked at and symmetric about 90° with respect to the beam direction in the centre of mass system.

The Br-Au collision pair was chosen such that the $1s$ atomic orbital binding energy of bromine approximately matched the binding energy of the $2s$ and $2p$ orbitals of gold. This should produce extensive ionization through electron promotion. This is seen in figure 2-5 where a schematic correlation diagram is shown. It is well known that there is a resonance for the production of $2p_1$ (1 denotes the lighter collision partner) vacancies (F. W. Saris, 1971) some of which may be radially coupled to the $1s$ orbital. Since the $3s\sigma$, $3p\sigma$, and $3p\pi$ levels are filled, the most probable excitation will be due to a $3d\sigma \rightarrow 3d\pi$ rotational interaction. It had been expected that if a bromine K vacancy ($1s_2$) were

carried into a second collision, MO L x-rays would be emitted.

The radiation produced by a 60 MeV ^{79}Br beam is shown in figure 4-1(a). The characteristic gold L x-rays and the bromine K x-rays are prominent and a radiation continuum may be seen which extends to at least 45 keV. However, the fact that the radiation is not MO x-rays is illustrated in figures 4-1(b), (c), and (d). Here the radiation shown was produced by beams of ^{12}C , ^{16}O and ^{35}Cl which have the same velocity as the ^{79}Br beam. Some of the most successful calculations of atomic ionization have been those based on the binary encounter model (M. Gryzinski, 1965) which treats the ionization as a two body Coulomb scattering of the bound target electrons by the nucleus of the projectile. The reason for using ions with the same velocity is that in the binary encounter approximation for vacancy production the extent of target ionization is then simply proportional to the square of the atomic number of the projectile. The slopes of the continua (exponentially decreasing with increasing photon energy) in figure 4-1 are very similar and between 22 and 35 keV drop to one-half intensity in 2.8, 2.8, 2.8 and 3.5 keV for carbon, oxygen, chlorine and bromine beams, respectively. Since the combined atomic number for the four systems changes from 85 for carbon on gold to 114 for bromine on gold, similar MO spectra are not expected. Not only should the maximum photon energy be different, the slopes must change drastically.

Figure 4-1

Unnormalized spectra for (a) 60 MeV ^{79}Br , (b) 26.6 MeV ^{35}Cl , (c) 12.1 MeV ^{16}O , (d) 9.1 MeV ^{12}C bombardment of a gold target. The horizontal axis presents the photon energy. The prominent peaks are L and K x-rays.

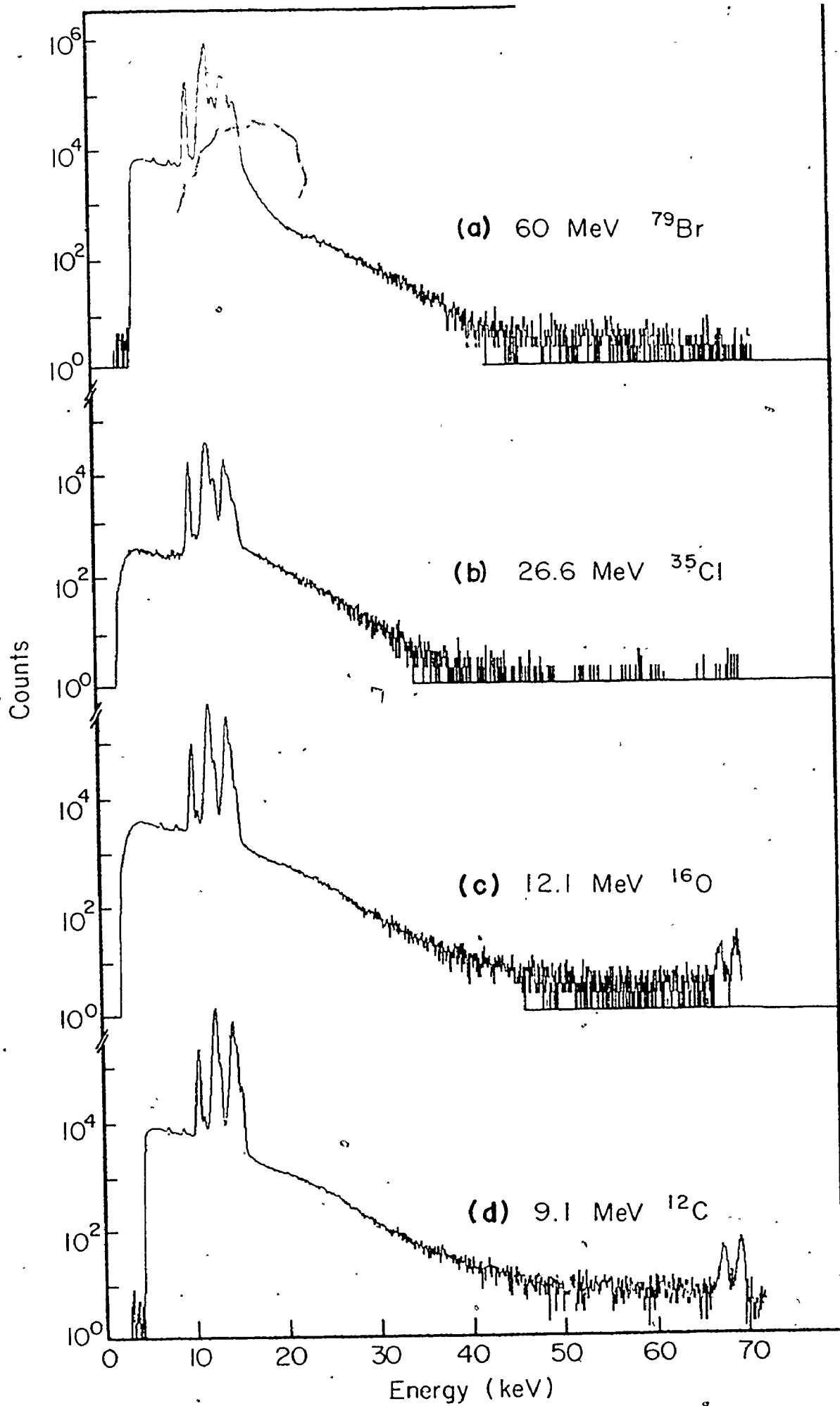


Table 4-1 shows a comparison of the production cross-sections. As is expected, the characteristic cross section increases rapidly with the atomic number of the projectile. However, the continuum radiation cross section from 22 to 35 keV divided by the number of characteristic target L x-rays is constant. This indicates that a major contribution to the continuum radiation is not dependent on the target-projectile combination, which would not be expected from a quasimolecular approach.

A number of explanations for this radiation have been considered and then rejected. The continuous nature of the radiation rules out the possibility of it being a result of characteristic x-rays and since the production cross section is not count rate dependent, it is not due to electronic pile-up. The bremsstrahlung from the projectile nucleus scattering off a target nucleus (K. Alder et al., 1956) is much too weak and does not have a strong enough dependence upon photon energy (Meyerhof, 1976). However, at sufficiently high energy this will become the dominant effect. Calculations, using the binary encounter approximation, of the bremsstrahlung radiation (F. Folkmann, 1974) emitted by secondary electrons slowing down in the target indicate that this effect is several orders of magnitude too small (even if the intensity is normalized to the intensity of the characteristic x-rays) (Meyerhof, 1976).

In the binary-encounter approximation one disregards during the collision all forces other than the Coulomb interac-

Table 4-1
Photon Cross sections

Projectile	Target L x-rays ^{a)}	Projectile K x-rays ^{a)}	Continuum ^{b)}	Ratio ^{c)}
Carbon	1.3		5.4×10^{-4}	4.1×10^{-4}
Oxygen	2.4		1.5×10^{-3}	6.5×10^{-4}
Chlorine	5.0		2.8×10^{-3}	5.6×10^{-4}
Bromine	150	120	6.2×10^{-2}	4.0×10^{-4}

- a) Cross section of characteristic x-rays in barns/sr
(\pm 40% error).
- b) Cross section of continuum x-rays from 22 to 35 keV
in barns/sr.
- c) Continuum x-ray cross section divided by target L
x-ray cross section.

tion between the nuclear projectile and the struck electron. At the moment of the collision the electron has velocity v_2 in the atom. If v_2 is assumed to be isotropically distributed, one can from the Rutherford cross section for the binary encounter calculate the average cross section for adding an energy ΔE to the kinetic energy E_2 of the electron. Consider an electron with binding energy U , and requiring that it leaves the atom with a kinetic energy E_e , then $\Delta E = U + E_e$. In order to calculate the energy spectrum for E_e one must integrate over a normalized velocity distribution of the electron in the atom. The resulting cross section for the emission of an electron with energy E_e is therefore calculable.

Bremsstrahlung may be emitted when the electron is ejected from the target atom. The electron can be treated as a light particle which is accelerated by the field of the incoming projectile and emits bremsstrahlung. An estimate of the cross section for electron ejection was calculated using the binary encounter approximation (M.E. Rudd et al., 1971) using the Fock velocity distribution of electrons for the different atomic shells (V. Fock, 1935). The bremsstrahlung was determined using classical electrodynamics (Jackson, 1962). The intensity is about three orders of magnitude too weak, although qualitatively it shows the correct photon energy dependence. This suggested mechanism was used in calculations

by Anholt and Saylor (1976) which verify the lack of intensity.

Another process which could contribute to the continua is radiative electron capture of target atom electrons to the K shell of the passing projectile (H. W. Schnopper et al., 1972). A target electron is captured into a projectile vacancy whereby a photon is emitted with an average energy $E_{REC} = E_c + E_k$, where E_c is the photon energy of the associated characteristic x-ray while E_k is the relative kinetic energy of the projectile atom and the electron to be captured. This results in a broadened peak (due to the electron velocity distribution) which extends only a few keV above the binding energy of the shell, whereas the continua extend many keV higher than the characteristic x-rays.

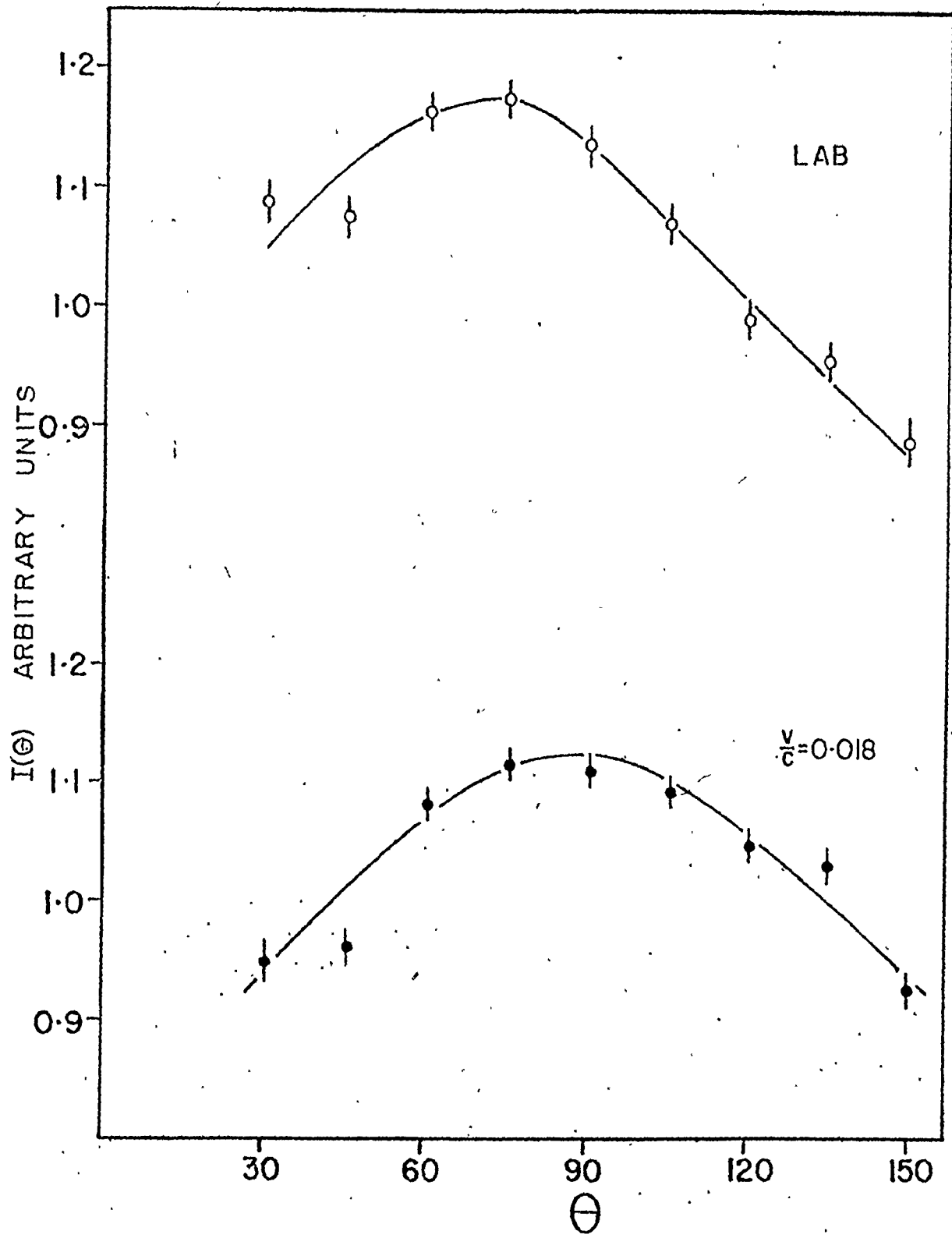
Finally, the maximum energy transfer to a gold atom by the low energy carbon beam is insufficient to bring a recoiling gold atom close enough to another gold atom to result in MO L x-rays from a Au-Au collision.

In order to learn more about the continua, an angular distribution of the photons produced with the bromine beam was measured from 30° to 150°. The characteristic x-rays were found to be isotropic to within 4%. However, as may be seen in figure 4-2, the radiation tail is anisotropic. The observation that the angular distributions are not symmetric about 90° as the MO picture suggests results from the fact that the

Figure 4-2

Angular distribution of 20 to 22 keV photons from a 60 MeV ^{79}Br bombardment of a thin gold target. The open circles represent the uncorrected data while data shown as the solid circles has been converted to the moving system assuming $v/c = 0.018$.





radiation is emitted by a moving system. This may be used to determine whether the source of radiation is from the bromine ion ($v/c = 0.04$), the combined bromine-gold system ($v/c = 0.012$) or energetic electrons ($v/c = 0.3$).

There are three factors which must be taken into account in converting the data to a moving system. Firstly, the energy of the photons will be Doppler shifted such that the energy in the moving (primed) system is given by (J. D. Jackson, 1962)

$$E' = \frac{\sqrt{1 - v^2/c^2} E}{1 + v/c \cos\theta}$$

where E is the energy in the laboratory frame of reference, v/c is the velocity in the lab relative to the velocity of light and θ is the laboratory angle.

Secondly, there will be an angular shift given by (J. D. Jackson, 1962)

$$\tan\theta' = \frac{\sqrt{1 - v^2/c^2} \sin\theta}{\cos\theta - v/c}$$

Finally, there must also be a correction made for the change in solid angle with which the detector observes the x-rays being emitted by the moving system.

$$\Omega' = \Omega \frac{1 - \frac{v^2}{c^2}}{\left(1 - \frac{v}{c} \cos\theta\right)^2}$$

where Ω is the solid angle in the laboratory frame of reference.

The effect of converting to a moving system, assuming a $v/c = 0.018$ is shown in figure 4-2. The experimental data only limit v/c to the range of $0.010 < v/c < 0.025$, but this is sufficient to show that the radiation is emitted during the collision.

In summary, it has been shown that radiation emitted during heavy ion-atom bombardment of Au has an intensity per Au L vacancy independent of the projectile and the slopes of the continua show little dependence on the atomic number of the combined system. However, the angular distribution of the continuum does show a symmetry about 90° in the centre of mass system just as MO model radiation would have. While MO radiation may contribute to the continuum region it must be concluded that other effects should be taken into account. Since the production of the radiation is not well understood, one must be careful when ascribing radiation continua to molecular orbital radiation.

CHAPTER 5

DOUBLE K-VACANCY STUDIES

5.1 Introduction

In heavy ion-atom collisions at medium energies (~ 0.7 MeV/amu), multiple inner-shell vacancies may be produced. If, for instance, both electrons are removed from the K-shell of either the target atom or the projectile atom during such an encounter, the holes created will be filled by the subsequent transitions of two electrons from higher-lying shells. Normally these jumps will be accompanied by the emission of two characteristic x-rays or the emission of two Auger electrons or one of each. However, it is also possible that both holes may be filled by a simultaneous transition of two electrons which results in the emission of a single photon with an energy greater than twice the normal K transition energy. The existence of this effect has been reported recently (Wölfel et al., 1975) with a subsequent experimental and theoretical upsurge in interest in this kind of process. A knowledge of the double vacancy production is required for an understanding of the hypersatellite ($K^{-2}L^{-n} + K^{-1}L^{-n-1}$), satellite ($K^{-1}L^{-n-1} + L^{-n-2}$) and two electron-one photon ($K^{-2}L^{-n} + L^{-n-2}$) transitions. The possibility that single x-ray emission of a multiple-vacancy state may be a contributing component to the x-ray continua also

was a motivating factor behind the present work. Multiple vacancies in the K-shell are among the easiest of any of the atomic shell vacancies to experimentally observe and are also relatively less complicated to understand theoretically.

A number of investigators have studied the emission of coincident K hypersatellite and KL satellite x-rays in doubly K-ionized atoms using radioactive sources (J. P. Briand et al., 1971; J. P. Desclaux et al., 1974; H. J. Nagy et al., 1975 and van Eijk and Wijnhorst, 1977). The probability per nuclear decay of producing a double K-vacancy is quite small ($\sim 10^{-5}$ in the best cases) which can result in the double vacancy coincidences being superimposed on a very large background. The background can be considerably reduced if a very weak source is used and if the experiment is run over a long period of time (van Eijk and Wijnhorst, 1977). In the present work the probability of double vacancy production is about two orders of magnitude greater than the source production probability and consequently resulted in a true-to-chance ratio of approximately one to one. Thus the experimental difficulties with background are reduced and the data reduction is simplified.

Richard et al. (1972) have studied the calcium hypersatellite structure resulting from the bombardment by 30 MeV oxygen ions. They detected the x-rays using a crystal spectrometer. A number of K_{α} hypersatellite lines were ob-

served which corresponded to calculated lines of different configurations of 2p vacancies.

In this present "in beam" study a beginning has been taken towards an understanding of the double K-vacancy processes during heavy ion-atom collisions at low velocities ($v_{\text{ion}}/v_{\text{K electron}} \ll 1$). Eighty MeV iodine ions from the FN tandem accelerator were used to bombard seven thin targets ranging in atomic numbers over the region of target-projectile symmetry ($Z_T \approx Z_P$), from silver ($Z = 47$) to lanthanum ($Z = 57$). Two coincident K x-rays were observed which may originate in the target atom, the projectile ion or from the holes being split between the target and projectile. The double vacancies studied have given information on the hypersatellite and satellite energy shifts, the sharing of double vacancies between the target and projectile atoms and the ratio of double vacancy production to single vacancy production. An insight into the production mechanisms involved has been achieved in attempting to explain the observed cross sections and the relative target and projectile vacancy intensities.

5.2 Satellite and Hypersatellite Structure

The x-rays which are observed in these heavy-ion atom collisions are emitted by atoms which are highly ionized. The equilibrium charge state of 80 MeV iodine projectiles passing through a solid target is twenty-three to twenty-five

(Betz, 1972). Since the emission may occur over a range of atomic configurations, the emitted x-ray lines from target and projectile atoms will be shifted to higher energy and will also be considerably broadened. If the two vacancies exist in the K-shell of an atom and an L-shell electron fills one of the K-vacancies then an x-ray may be emitted whose energy is increased from the normal x-ray since the nuclear shielding has been reduced. This x-ray is a hypersatellite x-ray. Now if another electron fills the remaining K-shell hole then a satellite x-ray may be emitted whose energy is intermediate between the normal and hypersatellite x-rays again due to the reduced screening of the nucleus since an L-vacancy is present.

For the sake of simplicity in the following discussion, the calculated K_{α} line in which only one vacancy in the atom is present, is called the diagram line while the "in beam" singles K_{α} line is called the normal K_{α} x-ray. Also the "in beam" satellite and hypersatellite lines are denoted by K_{α}^s and K_{α}^h , respectively.

The data from the coincidence experiments were stored on magnetic tape. In order to observe which x-rays are in coincidence, it is necessary to set a window about a specific energy region of one detector and then have the computer record all those events on the magnetic tape in the other detector in true prompt coincidence with this energy region. The

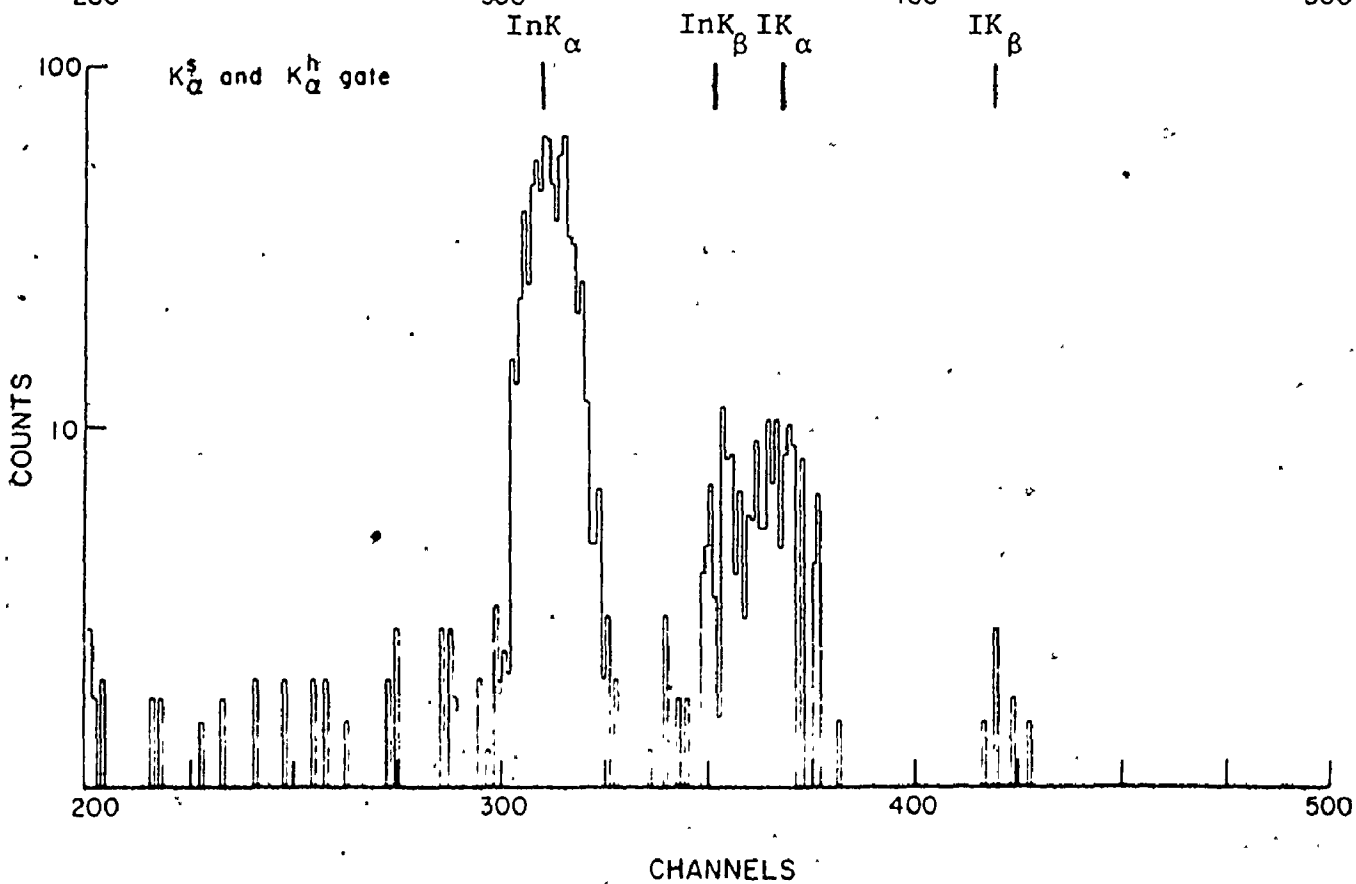
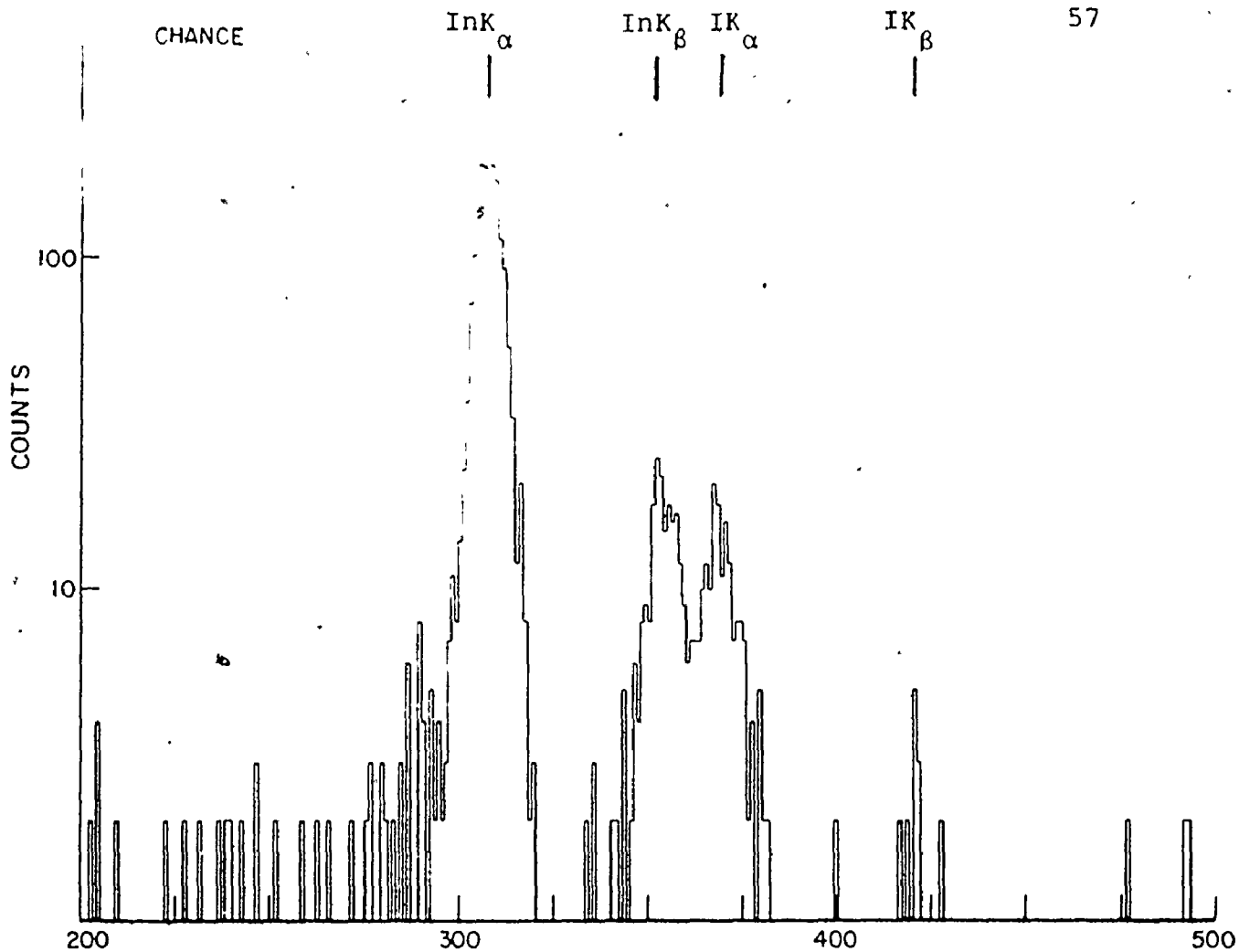
indium K_{α} satellite ($\text{In } K_{\alpha}^{\text{S}}$) and K_{α} hypersatellite ($\text{In } K_{\alpha}^{\text{h}}$) x-rays have been analyzed in just such a manner so that it may be determined which transitions are in coincidence with the K_{α}^{S} and K_{α}^{h} x-rays.

Figure 5-1 shows two spectra from the indium experiment; the upper plot displays the x-rays in the chance region of the time spectrum and effectively corresponds to a singles spectrum. The lower spectrum is a true prompt coincidence spectrum of all the lines in coincidence with the $\text{In } K_{\alpha}^{\text{S}}$ and K_{α}^{h} x-rays in the spectrum of the Ge(Li) detector. The spectra shown are coincidence events collected from the Si(Li) detector spectrum. The K_{α} peak in the lower plot is wider (≈ 970 eV FWHM) than the chance K_{α} peak (≈ 520 eV FWHM) due to the fact that it consists of both the K_{α}^{S} x-rays and K_{α}^{h} x-rays. The two x-ray peaks are not resolved by this experimental system but it has been determined by a least squares fit to the data that the two peak centroids are separated by approximately the FWHM resolution of the Si(Li) detector at this energy. It was also established by the same least squares fit that the intensities of the hypersatellite peak and the satellite peak are equal within the statistical uncertainty.

It might be expected that if a single projectile ion were to create K vacancies in two separate target atoms, as it passed through the target material that two normal K_{α} x-rays would be detected in coincidence. A K_{α} peak should appear

Figure 5-1

The upper graph is a plot of the Si(Li) detector coincidence events in the iodine on indium experiment from the chance background region of the time spectrum (see figure 3-5). The lower graph is a plot of the true prompt coincidence events of the Si(Li) detector in coincidence with the K_{α}^s and K_{α}^h x-rays of the Ge(Li) detector.



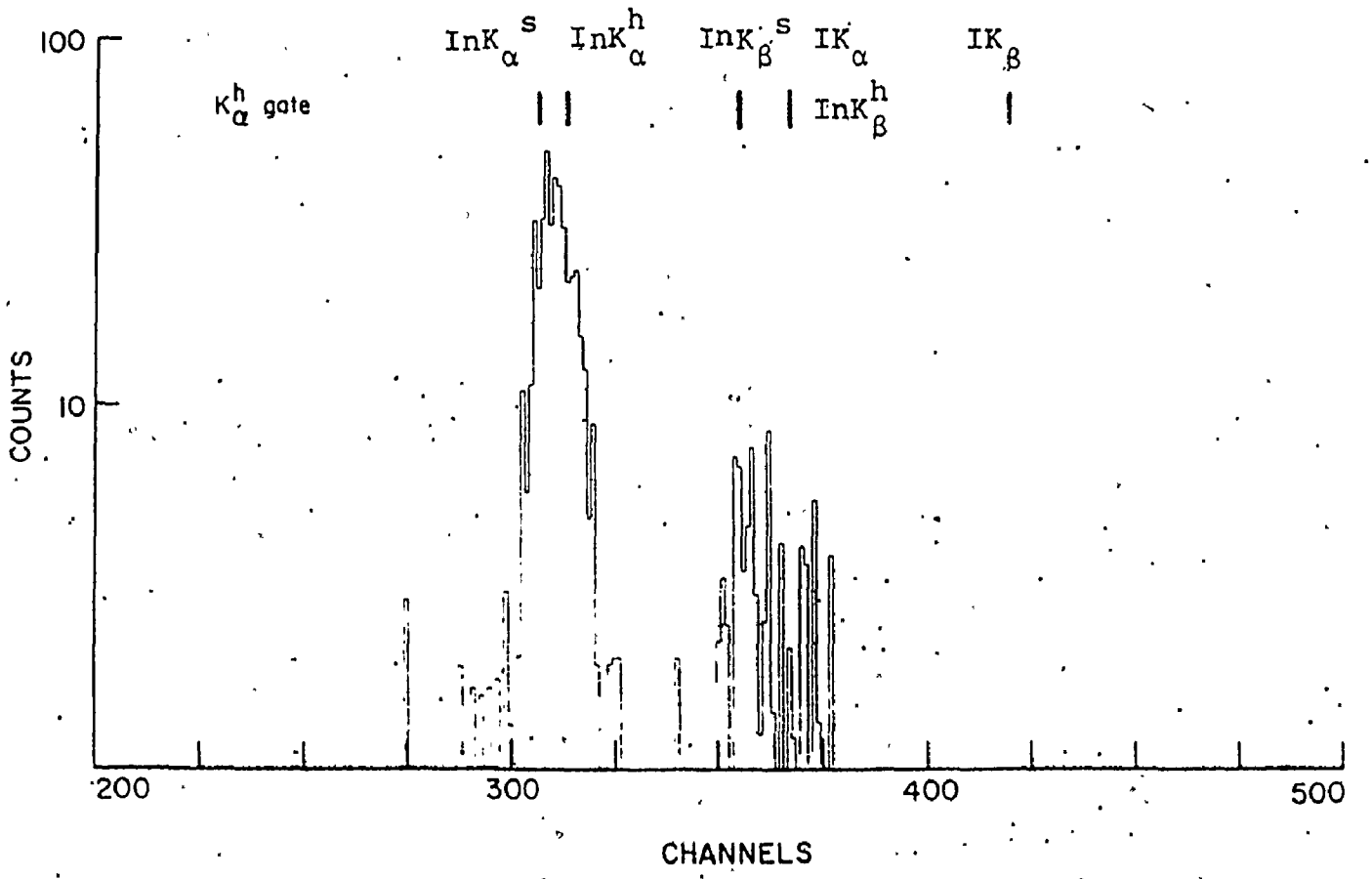
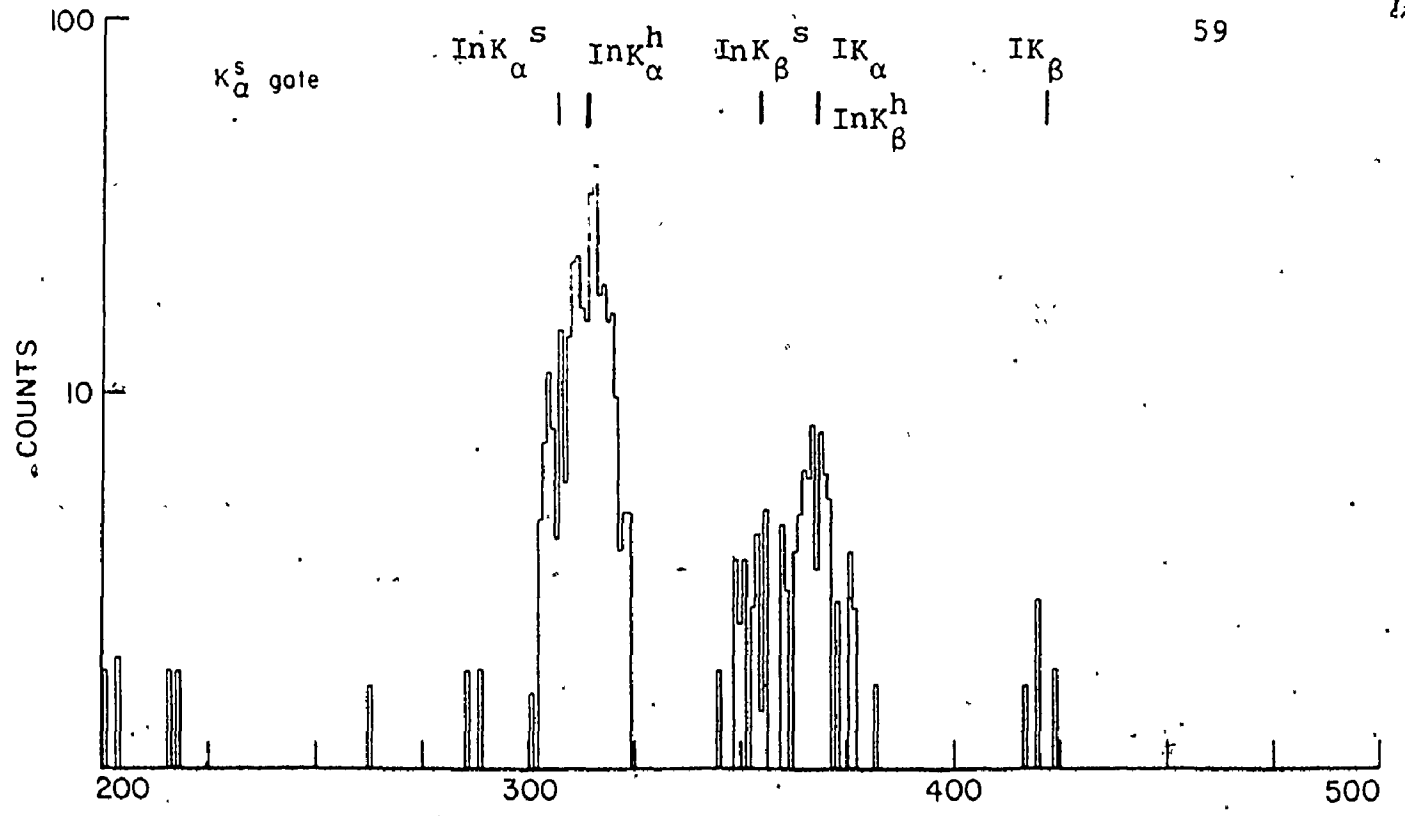
in the collected spectrum. The K_{α} line and the K_{α}^S line have approximately the same energy and so the K_{α}^S - K_{α} coincidences might appear as an enhancement of the K_{α}^S peak. Due to the statistical uncertainty a definitive statement cannot be made on this point, but at least it should be stated that the x-ray intensity from this process is much smaller than the double vacancy intensity.

An estimate of the ratio of production of two separate atom K vacancies to production of single K vacancies can be made if it is assumed that the probability for the two vacancies is the square of the single vacancy probability. The single K-vacancy cross sections (Meyerhof et al., 1977) and the target thickness are known which allow the single K-vacancy probabilities to be determined. The two separate K-vacancy intensity to single K-vacancy intensity ratio is proportional to target thickness so by keeping the targets thin the separate vacancy coincidences were effectively eliminated from this work. The calculated ratios for these experiments were approximately 10^{-5} which is two orders of magnitude lower than the double K-vacancy to single K-vacancy ratios measured.

Figure 5-2 shows the same data as in the lower plot of figure 5-1, but with windows set to illustrate the K_{α}^S and K_{α}^h structure. In the lower plot a window has been set on the right-hand side (the K_{α}^h side) of the indium K_{α} peak of

Figure 5-2

The upper graph is a plot of the true prompt coincidence events of the Si(Li) detector that are in coincidence with x-ray events of the Ge(Li) detector in the energy region encompassing the K_{α}^S x-rays. The lower plot is similar except the energy region is of the K_{α}^h x-rays.



the Ge(Li) detector spectrum. Thus the collected Si(Li) spectrum shows a skewed K_{α} peak because the K_{α}^h component has been suppressed due to the fact that two hypersatellite x-rays cannot be in true coincidence. Figure 5-3 is a map of which x-rays ought to be in coincidence, where the subscripts 1 and 2 designate the target and projectile atoms. Indium K_{α}^h x-rays are not expected to be in coincidence with the projectile iodine normal K_{α} or K_{β} x-rays, but are in coincidence with indium K_{β}^s x-rays. The lack of normal iodine x-rays in the plot illustrates this point.

The upper plot of figure 5-2 is the collected Si(Li) spectrum where a gate was set on the K_{α}^s -normal K_{α} side of the Ge(Li) indium K_{α} peak. The indium K_{α}^s and K_{β}^s lines are suppressed while the indium K_{α}^h and the normal iodine K_{α} and K_{β} x-rays are prominent. The indium K_{β} hypersatellite x-rays have about the same energy as the normal iodine K_{α} x-rays so they are lost in the much more intense iodine x-ray peak. The satellite and hypersatellite x-rays of iodine are not seen as is expected.

5.3 Energies of the X-rays

An experiment was conducted to determine the precise energy of the centroid of a singles K_{α} x-ray peak. This was accomplished by doing an experiment with the high resolution Si(Li) detector in which a target of tin was bombarded by the

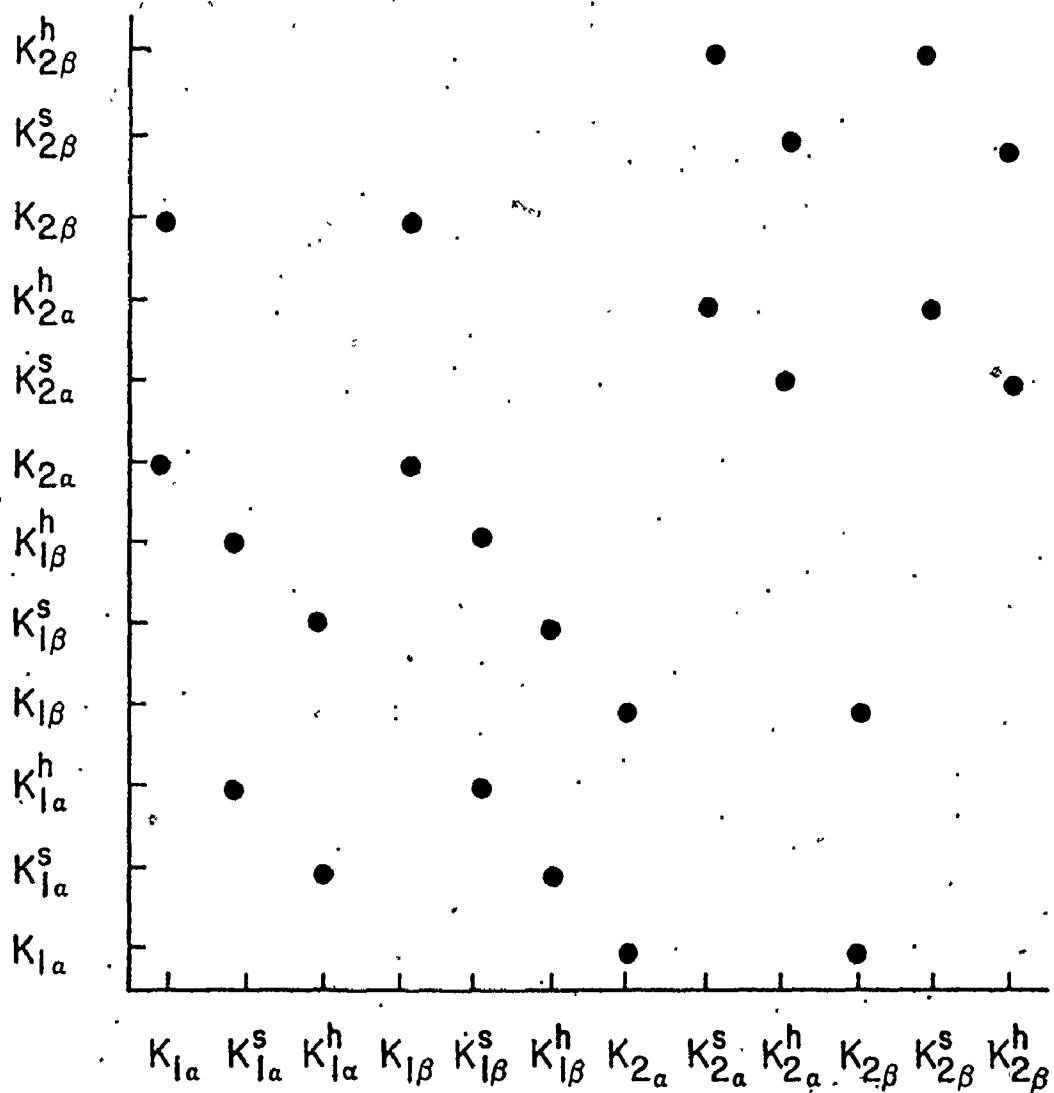


Figure 5-3

A schematic representation of K x-ray coincidences that may result from double K-vacancies. The numeral 1 represents one atomic species while 2 represents the other.

iodine beam. At the same time a molybdenum x-ray source and a ^{137}Cs source (emitting barium x-rays) were positioned such that the detector could see these sources as well as the tin "in beam" x-rays. By this method, x-rays of precisely known energies bracketed the tin x-rays whose energy was to be determined. A least squares fit to the data was done and an energy for the tin K_{α} x-ray line (weighted average of K_{α_1} and K_{α_2}) of 25.32 ± 0.05 keV, was determined. This is an energy 130 ± 50 eV greater than the averaged diagram line K_{α}^d (Desclaux, 1973).

This energy shift can be used to determine the mean state of ionization of the L shell when the transition occurred, that is to determine n in a vacancy configuration of $(1s)^{-1}(2p)^{-n}$. Richard (1972) has done a series of Hartree-Fock-Slater calculations for various configurations in which n varies from one to four. The systematics of the K_{α} and K_{β} x-ray energy shifts were calculated as a function of atomic number and the number of 2p vacancies, n . From this work it is estimated that the number of 2p vacancies for a 130 eV shift of the K_{α} x-ray for $Z=50$ is one to two vacancies. Unfortunately an accurate determination of the K_{β} energy shift is not possible since the tin K_{β} and the iodine K_{α} x-ray lines form an unresolved doublet peak in the spectrum.

The energy differences for the indium K_{α} diagram, normal, satellite and hypersatellite x-ray transitions are compiled in table 5-1. It is assumed here that the $K_{\alpha} - K_{\alpha}^d$ energy difference for indium is the same within errors as the measured tin energy difference. The K_{α}^h energy shift from the diagram line for indium has been measured from the decay of $^{114}\text{In}^m$ by means of a crystal spectrometer (van Eijk and Wijnhorst, 1977) and was found to be 566 ± 4 eV. A least squares fit to the peaks in the spectra of the in-beam experiment gives an energy difference of 529 ± 50 eV for $K_{\alpha}^h - K_{\alpha}$ which is in agreement with the spectrometer value. It is possible to make a direct comparison of this kind between these two difference values even though the in-beam experimental transitions have additional 2p vacancies involved. The reason for this is that the additional L vacancies have little influence on the energy difference between the K_{α} and K_{α}^h transitions. The energy shift of each of these transitions is the same for each additional L-shell vacancy present (Olsen and Moore, 1974).

5.4 Vacancy Sharing

The sharing of vacancies between the K shells of the partners in an atomic collision has been shown to follow a simple universal relationship (Meyerhöf, 1973). At infinite separation, the $2p\sigma$ state correlates with the 1s atomic state (see figure 2-6) of the lighter partner while the $1s\sigma$ state

Table 5-1

K Line X-ray Energy Differences in Indium
Coincidence Experiment

<u>Indium Transitions</u>	<u>Energy Difference</u>
$K_{\alpha} - K_{\alpha}^d$	$130 \pm 50 \text{ eV}$
$K_{\alpha}^h - K_{\alpha}^s$	500 ± 30
$K_{\alpha}^s - K_{\alpha}$	29 ± 35
$K_{\alpha}^h - K_{\alpha}$	529 ± 50
$K_{\alpha}^s - K_{\alpha}^d$	160 ± 70
$K_{\alpha}^h - K_{\alpha}^d$	660 ± 70

corresponds to the heavier collision partner $1s$ state. The derivation of the radial coupling transfer probability from the $2p\sigma$ state to the $1s\sigma$ state, W_{1s} (figure 5-4) is based on the charge transfer model of Demkov (1964).

Meyerhof has shown that the relationship between the K vacancy cross sections of the target, $\sigma_K(T)$, and the projectile, $\sigma_K(p)$, is given by

$$\frac{\sigma_K(T)}{\sigma_K(p)} = \frac{W_{1s}}{1-W_{1s}} = e^{-2x}$$

where x is defined as

$$x = \frac{\pi}{(2m_e)^{1/2} v} (I_T^{1/2} - I_p^{1/2})$$

m_e is the rest mass of the electron, v is the projectile velocity while I_T and I_p are the neutral-atom K binding energies of the target and projectile atoms, respectively (Desclaux, 1973).

In this study, the ratio of the target to projectile K-vacancy production intensities for all the targets used was determined and then compared to the above exponential relationship. The respective K_α line intensities from the chance spectra of the coincidence data were measured, then corrected for detector efficiency, for the K_α/K_β ratio and for fluorescence yield. The neutral-atom fluorescence yields were used in this correction (Bambynek, 1972). By taking the ratios of the cross sections, the errors associated with the corrections to the x-ray data are minimized. Figure 5-5

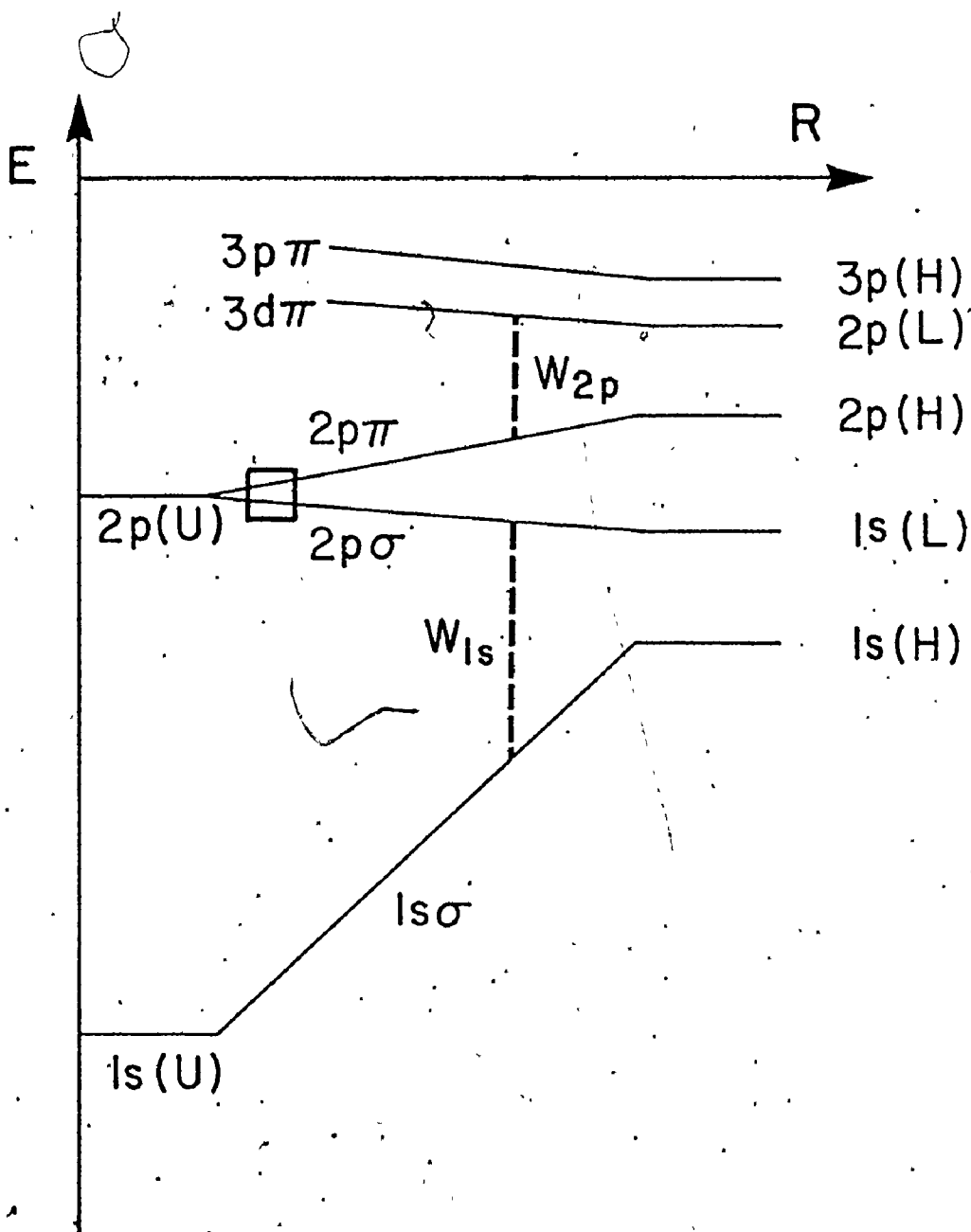


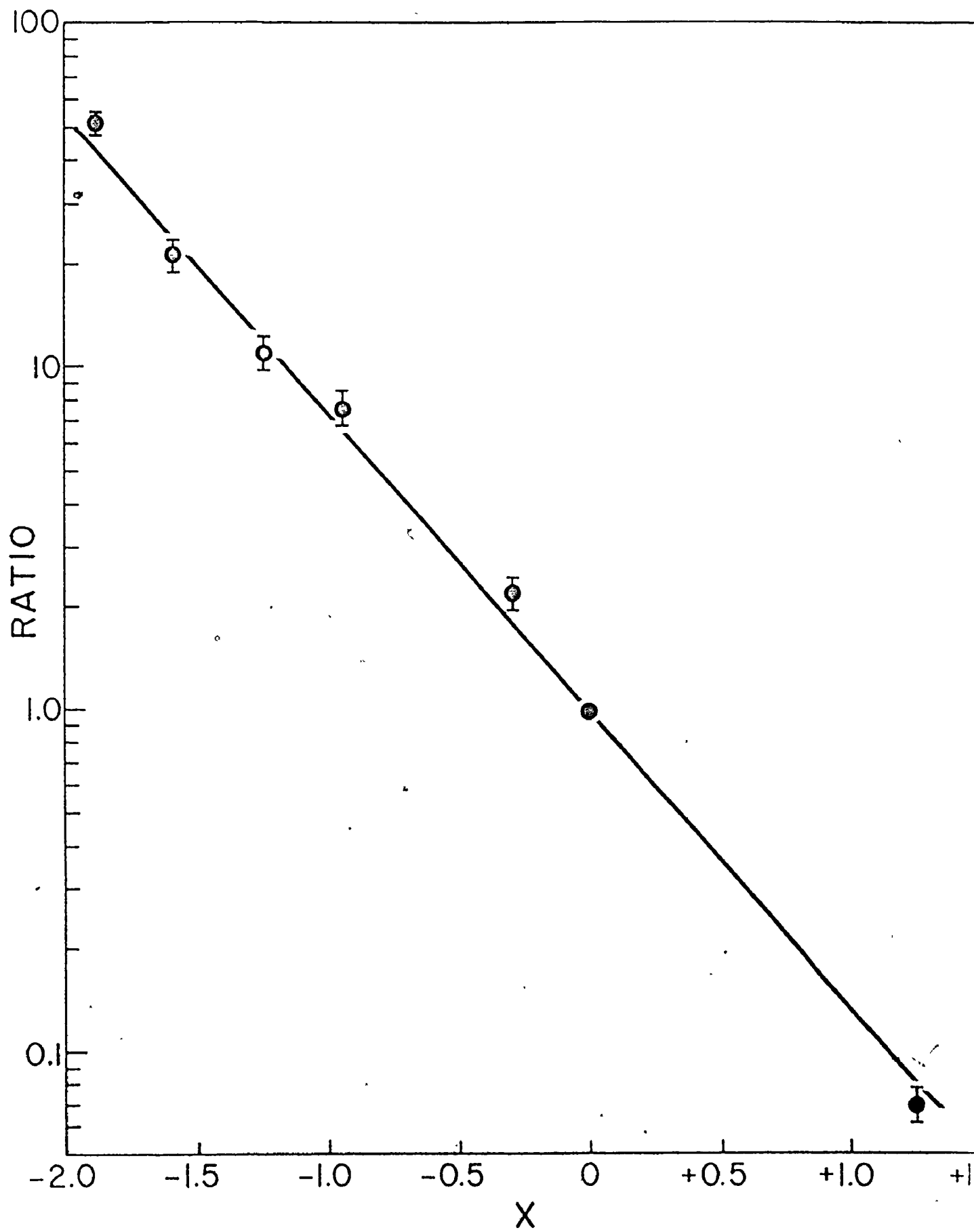
Figure 5-4

Schematic correlation diagram for an asymmetric collision between a lower-Z partner (L) and a higher-Z partner (H). Two radial coupling vacancy sharing processes are indicated, W_{2p} and W_{1s} . The region where rotational coupling may occur is indicated by the box.

11/2

Figure 5-5

A plot of the ratios of target to projectile single K-
vacancies produced by 80 MeV iodine beam bombardment of
the seven thin targets as a function of parameter x .
The line is a calculation of the ratio as $\exp(-2x)$.



shows that the calculated line fits the data well.

The double vacancy sharing has been determined also. For the single vacancy sharing case, the ratio of cross sections of the heavier atom to lighter atom is characterized by $W_{1s}/1-W_{1s}$. The cross sections may be expressed as

$$\sigma_1(H) \propto p_1 W_{1s}$$

$$\sigma_1(L) \propto p_1 (1-W_{1s})$$

where p_i is the probability of having i vacancies in the $2p\sigma$ state. Using a similar argument for two K-vacancies in one of the atoms and making the assumption that the two vacancies are independent of each other the double vacancy cross sections are (Briggs and Macek, 1972)

$$\sigma_2(H) \propto p_2 W_{1s}^2$$

$$\sigma_2(L) \propto p_2 (1-W_{1s})^2$$

However, under the action of sharing some of the double vacancies in the $2p\sigma$ state result in double vacancies in one atom and none in the other, while others produce simultaneous vacancies in both collision partners (Macek and Briggs, 1973). The expression for single vacancy production of this kind is given by

$$\sigma'_1(H) \propto p_2 W_{1s} (1-W_{1s})$$

$$\sigma'_1(L) \propto p_2 (1-W_{1s}) W_{1s}$$

Even though there are single vacancies in each atom

they will still of course result in coincident K x-rays. Since both the separated and the unseparated vacancies may result in coincident K x-rays, the total x-ray intensity for each atom is proportional to the sum of the double vacancy and shared double vacancy production.

$$\sigma_2^{\text{Total}}(\text{H}) = \sigma_2(\text{H}) + \sigma_1'(\text{H}) \propto p_2 W_{1s}$$

$$\sigma_2^{\text{Total}}(\text{L}) = \sigma_2(\text{L}) + \sigma_1'(\text{L}) \propto p_2 (1 - W_{1s})$$

The ratio of the heavier atom to lighter atom total K-vacancy cross sections using these expressions is simply $W_{1s}/(1 - W_{1s})$.

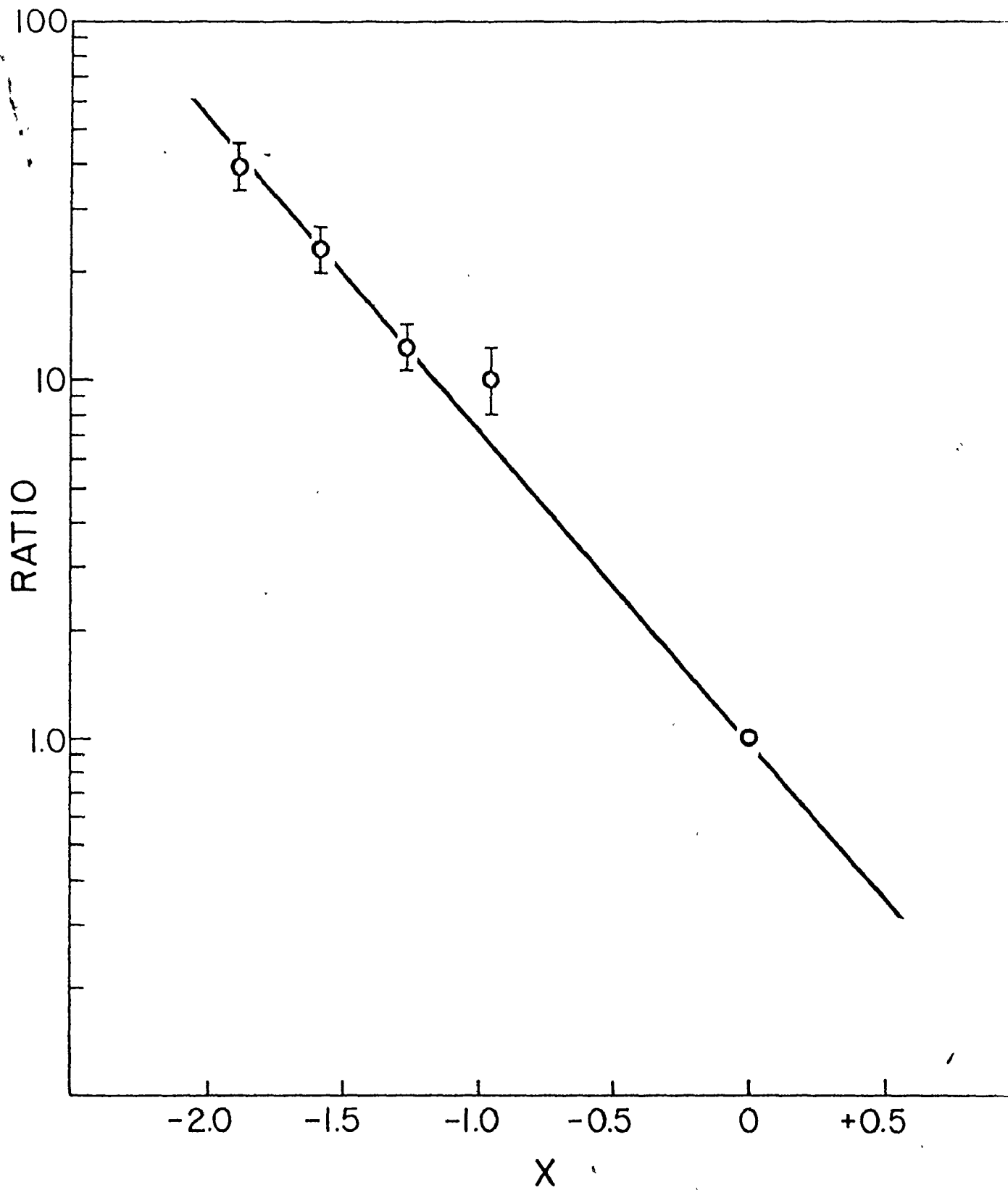
This is just the same as for the single K-vacancy case.

Figure 5-6 shows that the total double vacancy ratios indeed have the same dependence upon the parameter x as the single vacancy ratios. This appropriately corrected total vacancy production rate for a given atomic species was obtained from the total true prompt coincidence spectrum of each experiment. That is to say, all K x-rays in the energy spectrum of one of the detectors were gated on in order to collect the total vacancy production.

Unfortunately the resolution of the detector system precludes accurate measurements of the ratios of the double K-ionization in a single atom, which one would expect to be the square of the single vacancy ratios, that is $\exp(-4x)$.

Figure 5-6

Plot of the ratios of target to projectile double K-vacancy coincidence events as a function of parameter x . The line is the calculation of the ratio as $\exp(-2x)$.



Fortunately, the double vacancy work of Lennard et al. (1977a) has shown that this expression is in accord with their data and thus the assumption that the two holes act independently is substantiated.

5.5 Single K-vacancy Production

Before discussing the production of double K-vacancies, it is appropriate to consider the single K-vacancy formation for the symmetric collision region of heavy atoms, $Z_1, Z_2 \geq 10$. A remarkably good fit to the experimental K-vacancy cross sections has been obtained by Meyerhof et al. (1977) for symmetric and near symmetric collisions using a number of heavy-ion projectiles (e.g., figure 5-7). A two collision mechanism predominates in which a 2p-vacancy is prepared in the projectile in an initial collision. In a subsequent collision the vacancy is transferred to the $2p\sigma$ MO from the $2p\pi$ MO (see figure 5-4) via rotational coupling. The general form for the equation which gives the cross section is (Lennard et al. 1977b, Macek and Briggs, 1973).

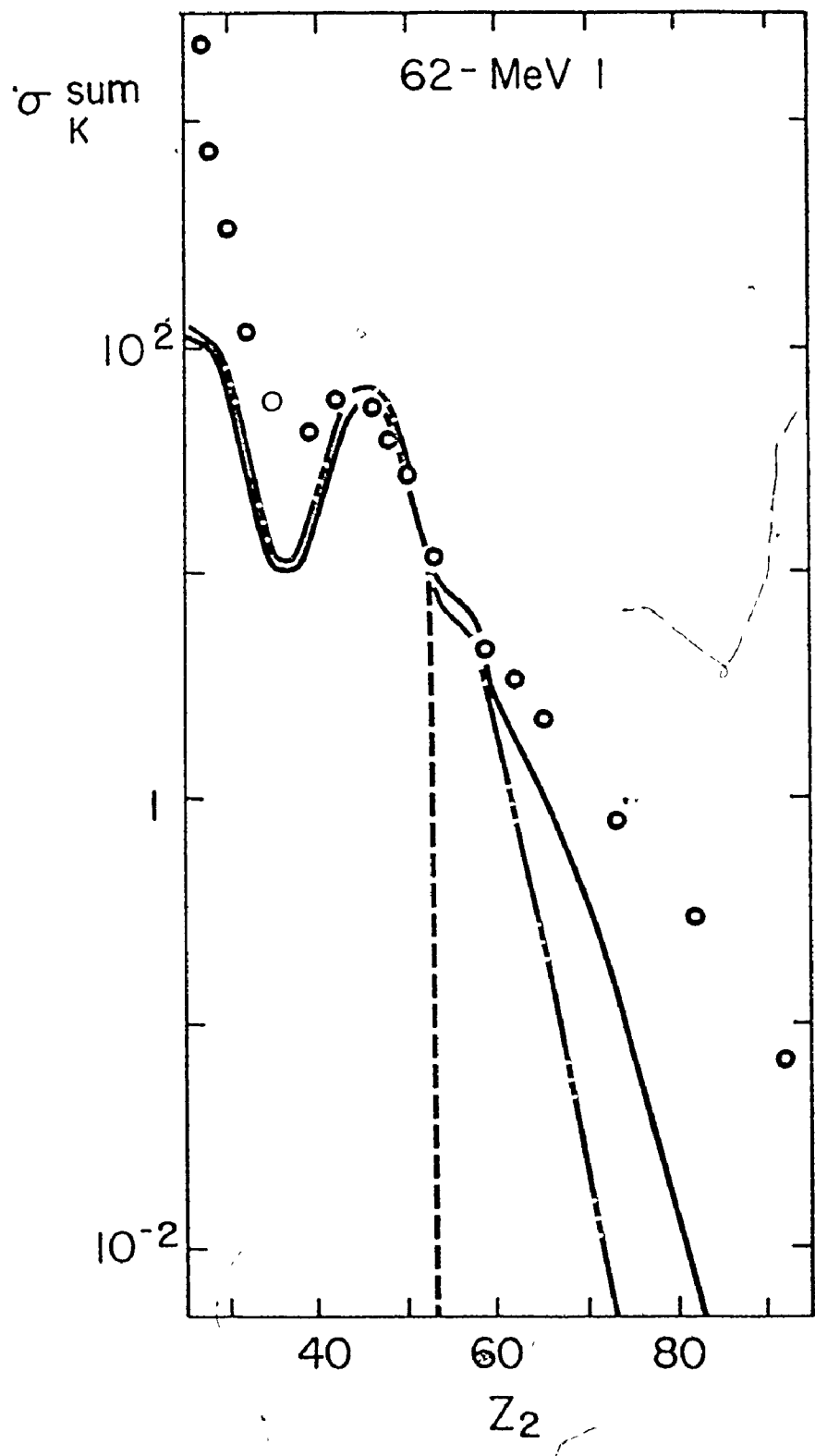
$$\sigma_{2p\sigma} = \frac{1}{3} N_{2p} W_{2p} \sigma_{rot}$$

The N_{2p} factor is the equilibrium number of 2p vacancies per projectile inside the target material. The approximation used by Meyerhof et al. for the projectile vacancy fraction is

$$N_{2p} = n_2 v_1 \tau_{1x} \sigma_{1x}^{2p}$$

Figure 5-7

The sum of target and projectile K-vacancy production cross sections for 62 MeV iodine as a function of the target atomic number. Solid curve represents the computed multiple-collision contribution to $2p\sigma$ cross section. Vertical dashed line indicates symmetry. The dot-dash line indicates a spin-orbit effect correction to calculation. For 80 MeV iodine collisions the spin-orbit effect is negligible (from Meyerhof et al., 1977).



where n_2 is the target atomic density, v_1 is the projectile velocity and τ_{1x} is the projectile x-ray lifetime for transitions from the atoms' M_{1V} and M_V levels to the L_{11} and L_{111} levels (Scofield, 1974) (see the appendix for explanation of notation). These levels were the only ones included because of the high state of projectile ionization. The cross section σ_{1x}^{2p} is the cross section for the production of projectile 2p x-rays. The product $n_2 v_1 \sigma_{1x}^{2p}$ is the mean number of vacancies per projectile per second which emit x-rays such that $\tau_{1x} n_2 v_1 \sigma_{1x}^{2p}$ is the steady state 2p vacancy number. It is interesting to compare the mean free time for the production of the 2p x-ray vacancies, $1/n_2 v_1 \sigma_{1x}^{2p}$, to the x-ray lifetime of the 2p vacancies. The mean free time for 80 MeV I ions in solid iodine is about 4×10^{-13} sec while the 2p x-ray lifetime is about 3×10^{-15} sec. Thus for each projectile ion with a 2p-vacancy it is relatively rare that it participates in a second collision.

W_{2p} is the 2p-vacancy sharing fraction. It has been shown by Lennard et al. (1977b) that if a projectile carries 2p vacancies into a collision then these vacancies are shared between the $2p\pi$ and $3d\pi$ MO's (figure 5-4) in a manner similar to the K-sharing between the $2p\sigma$ and $1s\sigma$ MO's.

$$W_{2p} = \frac{1}{1 + e^{1.79x_{2p}}}$$

where

$$x_{2p} = \frac{\pi}{(2m_e)^{1/2} v_1} (I_{2p}^{1/2}(T) - I_{2p}^{1/2}(P)) .$$

$I_{2p}(T)$ and $I_{2p}(P)$ are the 2p ionization energies of the target and projectile atoms, respectively. The factor of 1.79 was derived empirically.

The cross section σ_{rot} is the 2p σ -2p π rotational coupling cross section per incident 2p π_x vacancy. The cross sections along with the necessary scaling relationships have been calculated by Taulbjerg et al. (1976). Only the x-component of the 2p π state is coupled to the 2p σ state due to the nature of the rotation operator (see section 2.4). The factor of 1/3 is a statistical factor derived by Macek and Briggs (1973) which is the fraction of 2p vacancies that will be seen in the 2p π_x molecular orbital.

Thus K-vacancy production is felt to result from the equilibrium L-shell vacancies in the projectile being shared between the 2p π and 3d π orbits. Some of the 2p π vacancies are then coupled to the 2p σ orbital which in turn shares the vacancies with the 1s σ orbital. Consequently, because of the 1s σ MO being correlated with the 1s atomic orbital of the heavier partner and the 2p σ being correlated with the 1s atomic orbital of the lighter partner, vacancies exist in both collision atoms upon separation. The expression which describes the total K-vacancy cross section of both target and projectile is

$$\sigma_K = \frac{1}{3} n_2 v_1 \tau_{lx} \sigma_{lx}^{2p} W_{2p} \sigma_{rot}$$

All of the parts of the above equation for the cross section are calculable quantities, except the projectile 2p x-ray cross section which has to be determined experimentally. The iodine projectile 2p x-ray cross section was obtained from the 62 MeV iodine L x-ray data of Meyerhof et al. (1977) by multiplying the L x-ray cross sections by a factor of 0.9 (Datz et al., 1971). This factor is due to the fact that the L-shell contains 2s vacancies as well as the 2p vacancies. The 2p x-ray cross sections for 80 MeV iodine projectiles were determined by scaling the 62 MeV data to 80 MeV using the energy dependence of the L x-ray cross section, $\sigma_L \propto E^{0.8}$ (Stein et al., 1972).

5.6 Double K-vacancy Production

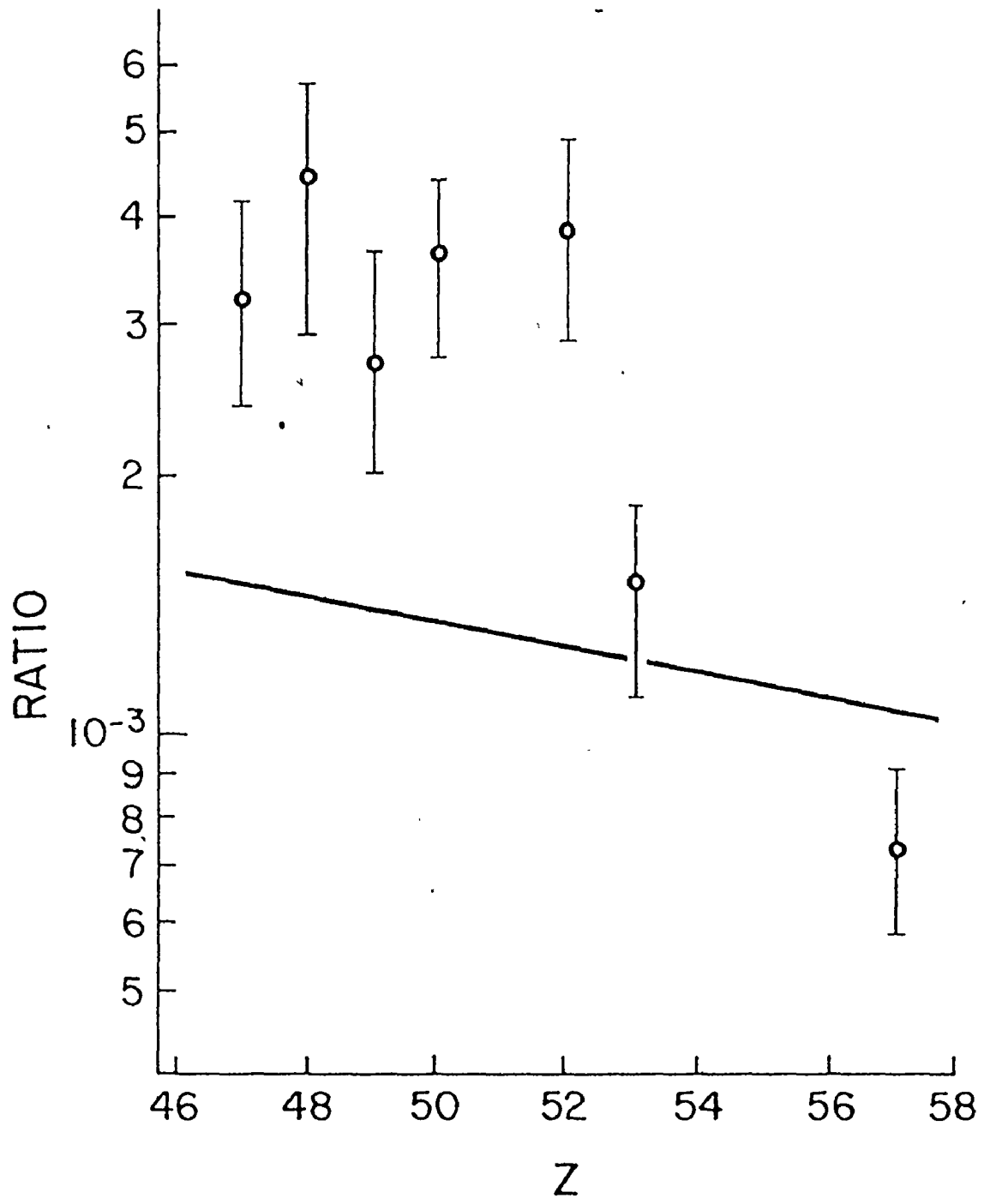
All double vacancy events whether from the target or the projectile or from a sharing of vacancies between target and projectile were collected in the analysis of the magnetic tape recordings of the experiments. This was accomplished by setting gates on the prompt time peak, on a background time region and on the energy region of one of the detectors containing all possible K x-rays. Thus the collected spectrum of the other detector contains all the information on the double vacancy events. The data were corrected for background chance events, for detector efficiency, for electronic efficiency, for solid angle and for fluorescence yield. The neutral-

atom fluorescence yields (Bambynek et al., 1972) were used to make the corrections since the fluorescence yield for double K-vacancy decay and the fluorescence yield for single K-vacancy decay are similar (Bhalla and Hein, 1973). The x-rays in the energy region of interest in these studies were not attenuated to a significant extent by either the target material or the thin plastic windows. Also the vacancy production as a function of projectile depth into the thin target does not change significantly because of projectile slowing since the velocity reduction of 80 MeV iodine ions in passing through the targets is about one percent (Northcliffe and Schilling, 1970).

The total number of double-vacancy events was obtained by summing all the K x-rays in the corrected spectrum of collected events. An appropriately corrected singles spectrum, from an experiment performed on the same target used in the coincidence experiment, was used to obtain the total single K-vacancy events. The number of K_{α} x-rays of the target or projectile atoms detected during each experiment by the detector common to both experiments was used to normalize the double vacancies events to single vacancy events. The ratio of total double vacancies created to total single vacancies created for seven target species by the bombardment of an 80 MeV iodine beam is shown as a function of atomic number in figure 5-8.

Figure 5-8

The experimental ratios of double $2p\sigma$ -vacancy to single $2p\sigma$ -vacancy production cross sections as a function of target Z for 80 MeV iodine projectiles. The line is a calculated ratio of the sum of double vacancy cross section calculations in the text ($\sigma_{2K}^a + \sigma_{2K}^b + \sigma_{2K}^c$) to the multiple collision $2p$ -vacancy cross section calculations.



Since the MO multiple collision model reproduces well the single K-vacancy cross section dependence on atomic number, it remains to calculate the double K-vacancy cross sections in order to obtain the double vacancy to single vacancy ratios to compare with the experimentally observed ratios. One mechanism is the MO multiple collision process as outlined in the previous section on single K-vacancy production. Another excitation mechanism is a direct Coulomb excitation process which will be considered specifically in its binary encounter approximation (BEA) formulation (e.g. McGuire and Richard, 1973).

The first model to be considered is one in which the single vacancy MO multiple collision approach is modified for the case of the two 2p-vacancies being brought from an initial collision into a subsequent collision during which the two vacancies are rotationally coupled to the 2p MO. The calculation of the equilibrium fraction of double 2p-vacancies was done using the prescription of Fortner and Garcia (1973) in which the equilibrium vacancy rate equations are solved for ionized projectiles passing through thin targets. The solution (assuming double electron processes are small) for the equilibrium fraction of projectiles with two 2p-vacancies is

$$\begin{aligned}
 N_{2p}^{(2)} &= n_2 v_1 \tau_{1x}^{(2)} \sigma_{1x}^{2p} N_{2p} \\
 &= n_2^2 v_1^2 \frac{\tau_{1x}^2}{2} (\sigma_{1x}^{2p})^2
 \end{aligned}$$

where the notation is as before except for the projectile x-ray double-vacancy lifetime, $\tau_{1x}^{(2)}$. This lifetime has been approximated as $\tau_{1x}/2$ following the statistical argument of Hopkins et al. (1976). The cross section for the production of two K-vacancies if the two 2p-vacancies are then rotationally coupled to the $2p\pi$ MO is given by

$$\begin{aligned}\sigma_{2K}^a &= \frac{1}{15} N_{2p}^{(2)} W_{2p}^2 \sigma_{2rot} \\ &= \frac{1}{15} n_2^2 v_1^2 \frac{\tau_{1x}^2}{2} (\sigma_{1x}^{2p})^2 W_{2p}^2 \sigma_{2rot}.\end{aligned}$$

The statistical molecular probability factor of 1/15 for the population of the $2p\pi_x$ MO is from the calculations of Macek and Briggs (1973). The sharing of two vacancies between the $2p\pi$ and $3d\pi$ MO's, W_{2p}^2 , was assumed to be simply the square of the single vacancy sharing. This idea is based on the assumption that the vacancies are independent of one another similar to the independence of the K-vacancies during the double K-vacancy sharing. The σ_{2rot} is the rotational coupling of two vacancies between the $2p\pi$ and $2p\sigma$ MO's as determined from the results of Taulbjerg et al. (1976). The results of the double K-vacancy cross section calculations for this mechanism are tabulated in table 5-2.

A second two-vacancy production mechanism is the direct Coulomb excitation of two K electrons. The impact parameter formulation of the binary encounter approximation

Table 5-2
X-ray Cross Sections*

Target atomic Number	σ_{2K}^a	σ_{2K}^b	σ_{2K}^c	σ_{1K}
47	4.9×10^{-2}	3.6×10^{-2}	4.9×10^{-2}	90.8
48	3.4	3.1	4.1	71.2
49	2.3	2.6	3.4	63.0
50	2.1	2.4	3.3	58.7
52	.85	1.6	2.2	36.8
53	.41	1.1	1.5	25.1
57	.12	.62	.84	12.1

* all cross sections are in units of barns

^a two projectile L-vacancy mechanism

^b single projectile L-vacancy, Coulomb excited $2p\pi$ -vacancy mechanism

^c single projectile L-vacancy, Coulomb excited $2p\sigma$ -vacancy mechanism

will be considered for this ionization. It is common to consider the scattering of particles as a function of impact parameters b and to express the total cross section as an integral over all impact parameters.

$$\sigma(V) = N \int_0^{\infty} 2\pi b P(V, b) db .$$

For the present case, $P(V, b)$ is the scattering probability per electron in a given shell and N is the number of participating electrons. McGuire and Richard (1973) have calculated the ionization probability $P(V, b)$ versus b using isotropic hydrogenic electron density distributions. The parameter V is a scaled velocity equal to v_i/v_o , where v_i is the velocity of the incident projectile and v_o is the orbital velocity of the atomic electron. Also there are scaling laws for the ionization probability which take into account the target and the projectile. $P(V, b)$ scales with projectile as Z^2 , the atomic number of the projectile. $P(V, b)$ scales with the target as Z_2^{-2} , where Z_2 is the effective nuclear charge seen by the projectile at the point of impact with the atomic electron. For the case of an L electron Z_2^2 may be taken from the Bohr atomic model as

$$Z_2^2 = 4|U_L|/13.6$$

where U_L is the binding energy of an L-shell electron in units of electron volts.

Now under conditions in which MO coupling mechanisms are not expected to contribute, the experimental data concerning single K-vacancy production in heavy-ion atom collisions has been described successfully in terms of a modified BEA direct Coulomb excitation (Foster et al., 1976). The binding energies used in this modified BEA model were the binding energies of the united atom rather than the binding energies of the target atom. This modification, though theoretically unjustified, resulted in a better agreement with the heavy ion atom collision data than the unmodified BEA calculation.

In light of the above considerations the double K-vacancy cross sections were calculated as

$$\sigma_{2K}(\text{BEA}) = \left[\frac{Z_1^2 13.6}{4U_{2p_{1/2}}(\text{UA})} \right]^2 \int_0^\infty 2\pi b P^2(v, b) db$$

where a numerical method based on the results of McGuire and Richard for the ionization probabilities was employed to evaluate the integral. The excitation is assumed to be of the electrons in the $2p_{1/2}$ shell of the united atom (following Foster et al.) which thus determines $U_{2p_{1/2}}(\text{UA})$ as well as the scaled velocity, V . The resulting cross sections that were determined are of the order of 10^{-4} barns, three orders of magnitude too low to give the experimentally observed ratio of double K-vacancies to single K-vacancies.

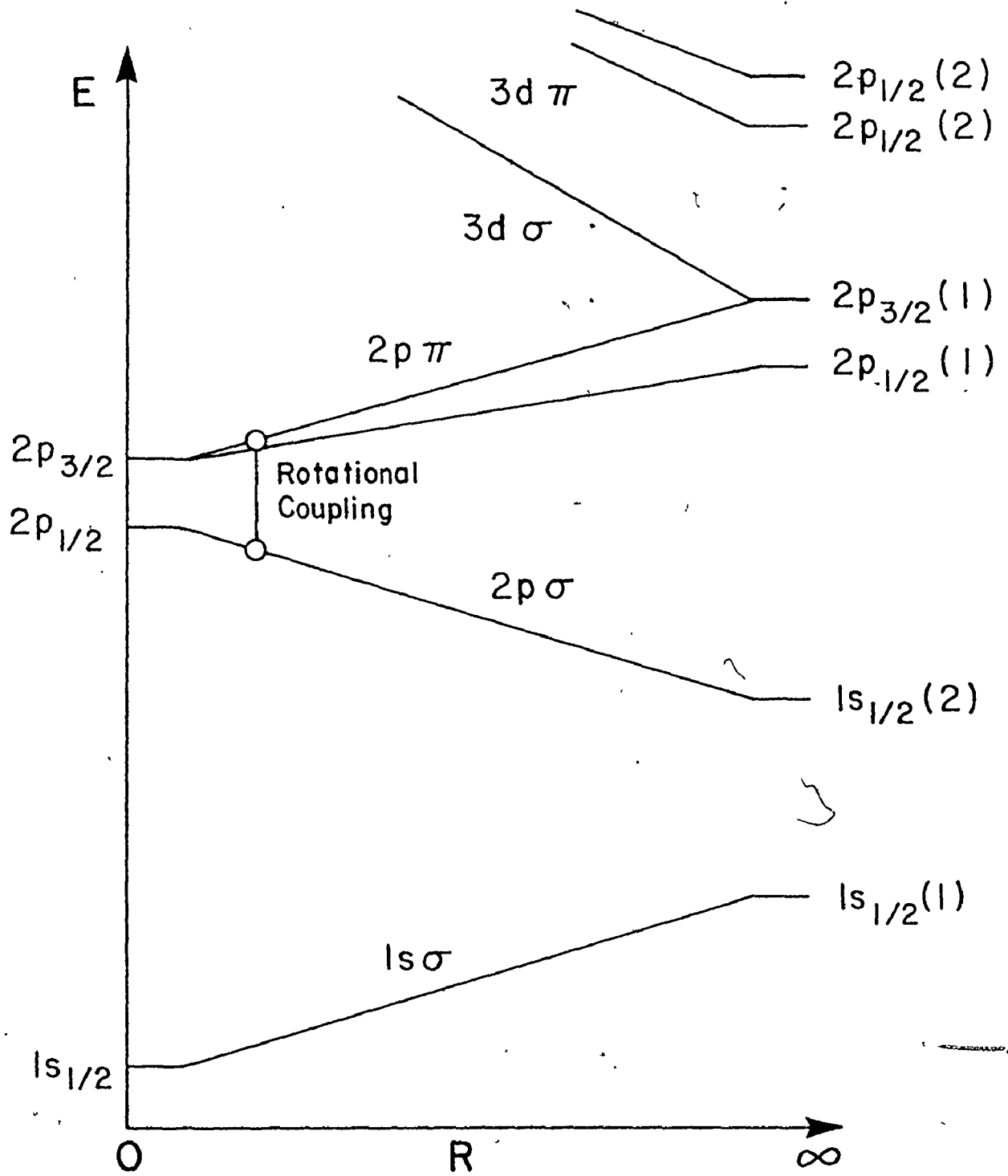
Another method that may produce two vacancies in the $2p$ MO is a direct Coulomb excitation of a $2p$ electron in a colli-

sion in which a MO coupled vacancy already exists. For this kind of two-vacancy production there exists two modes for the Coulomb excitation of a 2p electron. One way is an excitation of a $2p\sigma$ electron while the other possibility is that an electron in the $2p\pi$ MO may be excited. In the modified BEA formalism the two united atom levels $2p_{1/2}$ and $2p_{3/2}$ (which correspond to the $2p\sigma$ and $2p\pi$ MO's, respectively) were assumed to be degenerate. However, in the united atom limit where the combined atomic number is in the region of 106, the energy difference between the two states is approximately 8 keV (see figure 5-9). Consideration must therefore be given to possible excitations from either of the two levels.

First consider the direct Coulomb excitation of an electron from the $2p\pi_x$ MO in which a single MO vacancy already exists. Both vacancies are then coupled to the $2p\sigma$ MO. The formalism that has been chosen to express this excitation is the product of the multiple-collision MO mechanism which fits well the experimental single K-vacancy cross section data and the modified BEA mechanism which reproduces reasonably well the Coulomb excitation of inner-shell vacancies over a broad range of heavy ion-atom collisions. The rotational coupling aspect of the multiple-collision MO excitation mechanism is impact parameter dependent. Therefore in order to obtain a product of the cross sections of MO excitation and Coulomb excitation, the impact parameter representation of the BEA excitation of the $2p\pi_x$ electron was chosen. The

Figure 5-9

Schematic correlation diagram of some MO's of a heavy collision system. The numeral 1 represents the lower-Z separated atom while 2 represents the higher-Z partner. This illustrates $2p_{1/2}$ - $2p_{3/2}$ united atom splitting.



cross section for two vacancy production in the $2p\sigma$ MO may be represented as

$$\sigma_{2K}^b = \frac{1}{3} n_2 v_1 \tau_{1x} \sigma_{1x}^{2p} W_{2p} \int_0^{\infty} 2\pi b P_{rot}^2(b) P_{2p\pi}(b) db$$

where $P_{2p\pi}(b)$ represents the appropriately scaled BEA ionization probability and $P_{rot}(b)$ represents the $2p\pi$ - $2p\sigma$ rotational coupling probability from the results of Taulbjerg et al. (1976). The results of the double vacancy cross section calculations for this mechanism are tabulated in table 5-2.

Next consider the process of the Coulomb excitation of a $2p\sigma$ electron and the vacancy in the $2p\pi_x$ MO being coupled to the $2p\sigma$ MO. The cross section for this process is

$$\sigma_{2K}^c = \frac{1}{3} n_2 v_1 \tau_{1x} \sigma_{1x}^{2p} W_{2p} \int_0^{\infty} 2\pi b P_{rot}(b) (1 - P_{rot}(b)) P_{2p\sigma}(b) db$$

where the $P_{rot}(b)$ probability takes into account the coupling of the $2p\pi_x$ vacancy while the $1 - P_{rot}(b)$ term is the probability that the Coulomb excited $2p\sigma$ vacancy is not coupled to the $2p\pi_x$ MO. Once again the results of these double vacancy cross section calculations are tabulated in table 5-2. Also listed in table 5-2 are the MO multiple collision single K-vacancy cross section results, σ_{1K} .

If the three cross sections as determined for each target are simply summed, then the resultant total cross section is a classical calculation. The ratios of the summed

double K-vacancy cross sections to the single K-vacancy MO multiple collision cross sections are plotted as a solid line in figure 5-8. The calculated ratios are of the right magnitude but do not have as strong an atomic number dependence as the experimental ratios. Nevertheless, the calculated ratios decrease with increasing atomic number as they should.

A few comments ought to be given on the double K-vacancy cross section calculations. Other possible modes of excitation have not been included such as the rotational coupling of the $2p$ MO to higher-lying MO's (e.g. see review by Taulbjerg and Meyerhof, 1977). Also not included is the dynamic rotational coupling of the $2p\pi_x$ MO to higher-lying MO's which may increase the number of $2p\pi_x$ vacancies that can be coupled to the $2p\sigma$ state. The approximation that the united atom energies of the $2p_{1/2}$ and $2p_{3/2}$ levels represent the energy regime where the Coulomb ionization takes place may not be appropriate. In particular the scaling of the ionization probabilities $P_{2p\pi}(b)$ and $P_{2p\sigma}(b)$, and v_0 the orbital electron velocity are strongly affected by the energies of the levels. At the values of the scaled velocity $V (v_i/v_0)$ used in the present calculations, the BEA cross section is changing dramatically. Consider also that the three calculated cross sections were simply added together to give the total $2K$ -vacancy cross sections. This may not be valid since there may be coherent interference among the three modes of production,

particularly between the σ_{2K}^b and σ_{2K}^c ionization probabilities which because of their similar magnitudes could result in a significant variation from the summed values.

5.7 Double L-vacancy Calculation

The preceding calculations approximate the double K-vacancy production cross section intensities reasonably well. However, the atomic number dependence of the double to single K-vacancy ratio is not well explained. In the calculation of the σ_{2K}^a cross section (the two L-shell vacancy MO mechanism) the assumption was made that double electron excitation processes are small relative to single electron excitation and thus the double L-vacancy was considered to be produced in two separate collisions. In this section a calculation of the double to single K-vacancy ratio is made using a model which considers the double L-vacancy as being produced in a single collision. The cross-section for the process is treated as a free parameter.

In this model two 2p-vacancies are prepared in the projectile. In a subsequent collision the two 2p-vacancies are rotationally coupled from the $2p\pi$ MO to the $2p\sigma$ MO. The general form of the cross section will be

$$\sigma_{2p\sigma}^{(2)} = \frac{1}{15} N_{2p}^{(2)} W_{2p}^2 \sigma_{2rot}$$

where, as previously, $1/15$ is the molecular probability factor

(Macek and Briggs, 1973), W_{2p}^2 is the vacancy sharing fraction between the $2p\pi$ and $3d\pi$ MO's and σ_{2rot} is the rotational coupling of the two vacancies between the $2p\pi$ and $2p\sigma$ MO's (Taulbjerg et al., 1976).

The $N_{2p}^{(2)}$ factor is the equilibrium number of two 2p-vacancies per projectile inside the target material. This is given by

$$N_{2p}^{(2)} = n_2 v_1 \tau_{1x}^{(2)} \sigma_{1x}^{2p(2)}$$

where n_2 is the target atomic density, v_1 is the projectile velocity and $\tau_{1x}^{(2)}$ is the projectile x-ray double-vacancy lifetime. As before $\tau_{1x}^{(2)}$ is assumed to be $\tau_{1x}/2$. The double K-vacancy production cross section for this double L-vacancy multiple collision MO mechanism is given by

$$\sigma_K^{(2)} = \frac{1}{15} n_2 v_1 \frac{\tau_{1x}}{2} \sigma_{1x}^{2p(2)} W_{2p}^2 \sigma_{2rot}$$

The total single K-vacancy production cross section is

$$\sigma_K = \frac{1}{3} n_2 v_1 \tau_{1x} \sigma_{1x}^{2p} W_{2p} \sigma_{rot}$$

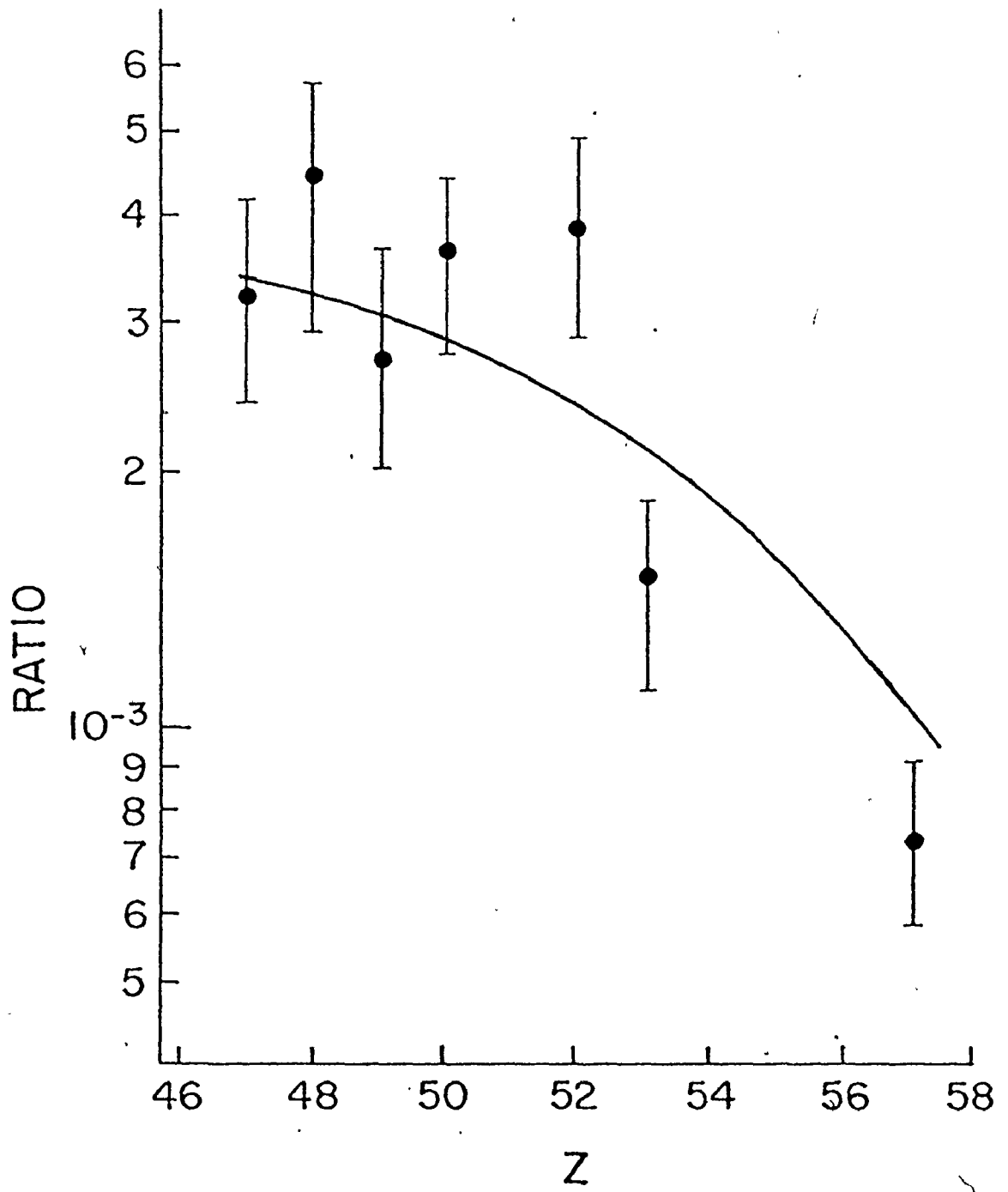
Therefore the ratio of these cross sections is given by

$$\frac{\sigma_{2K}^{(2)}}{\sigma_K} = \frac{1}{10} W_{2p} \frac{\sigma_{2rot}}{\sigma_{rot}} \frac{\sigma_{1x}^{2p(2)}}{\sigma_{1x}^{2p}}$$

A best fit of this calculation to the data is shown in figure 5-10 assuming the double to single 2p-vacancy cross section ratio is a constant with a value of 0.10. The calculation fits

Figure 5-10

Plot of the ratio of double to single K-vacancies as a function of atomic number. The line is a calculation of the ratios using the double L-vacancy calculations assuming $\sigma_{1s}^{2p(2)}/\sigma_{1x}^{2p} = 0.10$.



the data well in that the target atomic number dependence is reproduced. The model also suggests that the probability of exciting two L-shell electrons is 1/10 of the probability of exciting a single electron. This double 2p-vacancy cross-section contains a statistical factor of five relative to the single 2p-vacancy cross section since there are 6 electrons that may be singly excited while there are 6 times 5 ways that a double 2p-vacancy excitation may occur.


CHAPTER 6

SUMMARY

The work presented in this thesis consists of two studies of aspects of photon radiation emitted during the collision of heavy-ion projectiles on thin foils of heavy atoms. The continuum studies were performed at the time when interest was growing in the nature of the continuum x-rays produced in the accelerator-based experiments on heavy ion-atom collisions. Molecular orbital radiation from the quasimolecules formed during the collision was the theoretical framework for the understanding of the continuum photons that were emitted. The transient molecular orbital approach was also the basis of the theoretical calculations for double K-ionization which was the other aspect of collisionally induced x-ray emission studied.

The continuum studies are of note since they showed that continuum spectra exist for quite asymmetric collision systems as well as for collisions between symmetric or near symmetric partners. By obtaining an angular distribution of the continuum radiation emitted, it was possible to show that the emission occurred during the collision. A number of theoretical approaches were attempted in order to determine the production mechanism for these continua but none was found that

satisfactorily explained both the overall intensity and the intensity dependence upon photon energy that was observed experimentally. Experiments of greater sophistication such as coincidence experiments involving photons, electrons and ions are needed to unravel the production mechanisms involved. However, these kinds of experiments are extremely difficult due to the high backgrounds of electrons and photons resulting from the large atomic ionizations present in the collision.



The double K-vacancy production studies are the first to be published of their kind. The work represents a different approach to the experimental observation of multiple vacancies since previously work on in-beam collision production has been performed using crystal spectrometers. Although the solid state detectors do not have the resolving power of the crystal spectrometers the coincidence technique has made possible the direct measurement of double K-vacancies and allowed the observation of the sharing of the vacancies between the projectile and target atoms. The double vacancies produced may be shared between the colliding atoms or one of the two atoms may have both of the vacancies. The ratio of all vacancies of one atom species to all vacancies of the other atomic species has been determined in this work and in conjunction with the single photon-two electron transition work of Lennard et al. (1977a) verifies the essential independence of the vacancies during the sharing process.

The ratio of double K-vacancies to single K-vacancies has been determined for collisions of 80 MeV iodine on seven target atomic species in the region of symmetry with iodine. Since the single K-vacancy production cross sections can be calculated using the multiple collision molecular orbital model, the double K-vacancy production cross section was calculated using this approach. The ratios of these two cross section determinations are low by a factor of approximately eight from the observed ratio. Other mechanisms have been considered such as the Coulomb excitation of the electrons from the united atomic orbitals. The BEA formalism used gives a reasonable qualitative agreement with a large body of data but often the quantitative calculations are in poor agreement with observed cross sections (Foster et al., 1976). Nevertheless, it is one of the better impact parameter formulations. A hybrid model of double vacancy production involving the MO and BEA excitations has also been implemented to calculate the cross section. Individually, these approaches do not explain the intensities observed nor does a sum of the mechanisms satisfactorily reproduce the experimental data. The summed intensity determination gives approximately the observed intensity but does not exhibit a strong enough dependence on atomic number.

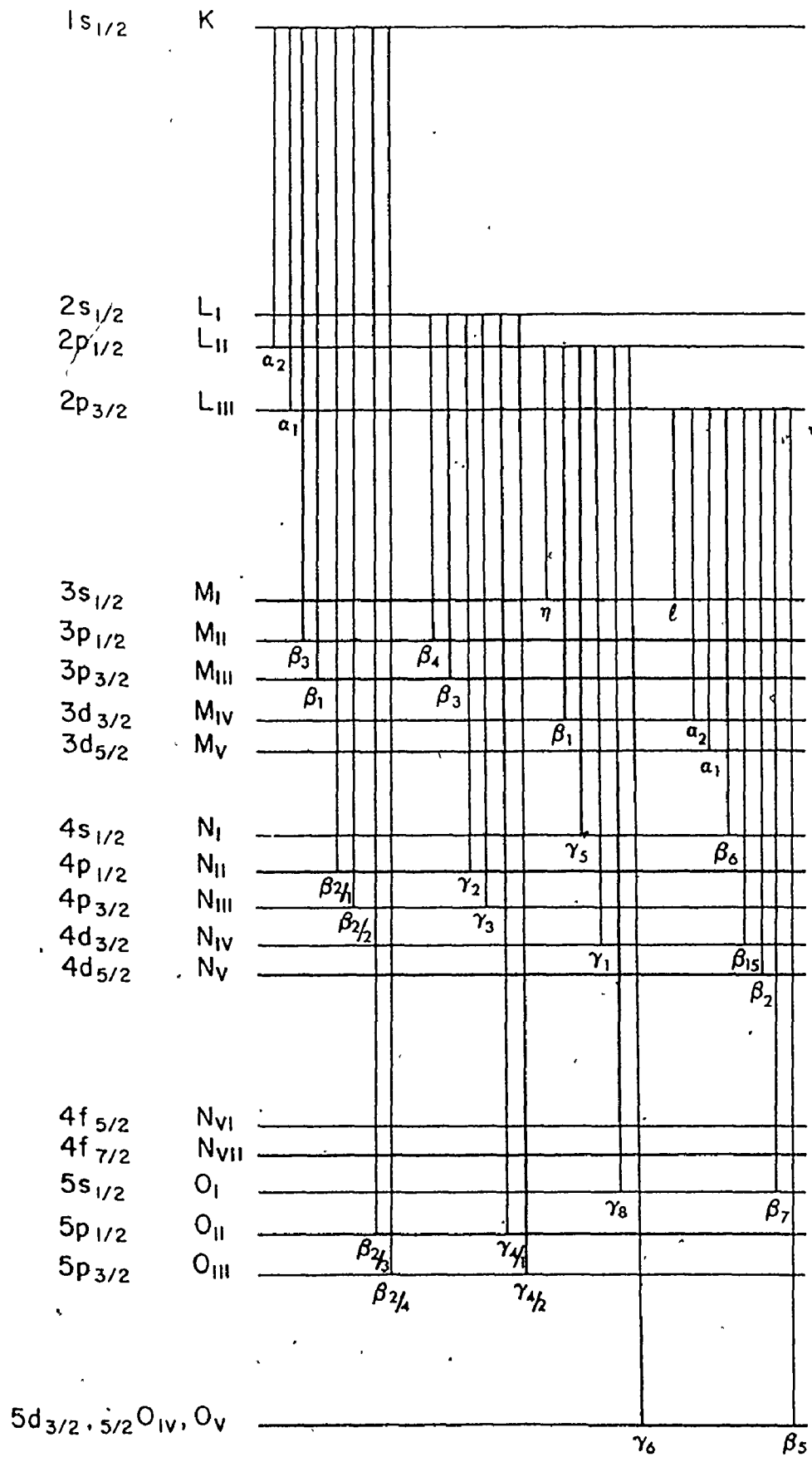
A more fundamental approach to the double excitation process is indicated by the failure of the models to account for the observed intensities and Z-dependences. More experimental study is required to determine the nature of the exci-

tation mechanism. Experimental determinations of the dependence of the double to single vacancy ratios on projectile energies, on projectile atomic number and on target atomic number are necessary to achieve a basic understanding. Also, the double vacancy dependence on target atomic density and on target thickness is required to determine the single or multiple collision nature of the excitation process.

The other approach to the problem of determining the double to single K-vacancy ratios was to assume that double L-electron excitation is responsible for double K-vacancy production. The proposed mechanism for the transfer of two L-vacancies to the $2p\sigma$ MO of the transient quasimolecule was similar to the single K-vacancy multiple collision MO mechanism. The result of following this prescription was that the atomic number dependence of the double to single K-vacancy ratio was reproduced and the ratio of double to single L-vacancy cross sections was found to be approximately 0.1. This one free parameter approach may be a better model than the direct calculation of the double K-vacancy approach since the atomic number dependence is reproduced. The problem remains however of calculating the double electron excitation process which results in two vacancies being transferred to the K-shells of the collision partners.

APPENDIX

A schematic representation of the atomic levels and the notations used to describe the levels. The Siegbahn notation is used to identify the atomic transitions which fill K and L shell vacancies.



REFERENCES

- K. Alder, A. Bohr, T. Huus, B. Mottelson and A. Winther, Rev. Mod. Phys. 28 (1956) 432.
- P. Armbruster, E. Röckl, H.J. Specht and A. Vollmer, Z. Naturforsch., 19A (1964) 1301.
- R. L. Auble, Nuc. Data Sheets 7 (1972) 465.
- W. Bambynek, B. Craseman, R. W. Fink, H. U. Freund, H. Mark, C. D. Swift, R. E. Price and P. V. Rao, Rev. Mod. Phys. 44 (1972) 716.
- M. Barat and W. Lichten, Phys. Rev. A6 (1972) 211.
- H. D. Betz, Rev. Mod. Phys. 44 (1972) 465.
- C. P. Bhalla and M. Hein, Phys. Rev. Lett. 30 (1973) 39.
- J. P. Briand, P. Chevallier, M. Tavernier and J.P. Rozet, Phys. Rev. Lett. 27 (1971) 777.
- J. S. Briggs and J. Macek, J. Phys. B: Atom. Molec. Phys. 5 (1972) 5.
- W. M. Coates, Phys. Rev. 46 (1934) 542.
- S. Datz, C. D. Moak, B. R. Appleton and T. A. Carlson, Phys. Rev. Lett. 27 (1971) 363.
- C. K. Davis and J. S. Greenberg, Phys. Rev. Lett. 32 (1974) 1215.
- Yu. N. Demkov, Sov. Phys. JETP 18 (1964) 138.
- J. P. Desclaux, At. Data and Nuc. Data Tables 12 (1973) 312.
- J. P. Desclaux, Ch. Briançon, J. P. Thibaud and R. J. Walen, Phys. Rev. Lett. 32 (1974) 447.
- R. D. Evans, "The Atomic Nucleus" (McGraw Hill), 1955, p. 838.
- U. Fano and W. Lichten, Phys. Rev. Lett. 14 (1965) 62.
- B. Fastrup, G. Hermann and K. J. Smith, Phys. Rev. A3 (1971) 1591.
- V. Fock, Z. Physik 98 (1935) 145.
- F. Folkmann, C. Gaarde, T. Huus and K. Kemp, Nucl. Instr. Methods 116 (1974) 487.

- R. J. Fortner and J. D. Garcia, in Atomic Collisions in Solids, ed. Datz, Appleton and Moak (1975) 469.
- C. Foster, T. P. Hoogkamer, P. Woerlee and F. W. Saris, J. Phys. B: Atom. Molec. Phys. 9 (1976) 1943.
- B. Fricke, K. Rashid, P. Bertoncini and A. C. Wahl, Phys. Rev. Lett. 34 (1975) 243.
- J. D. Garcia, Phys. Rev. A1 (1970) 280, 1402.
- J. D. Garcia, R. J. Fortner and T. M. Kavanagh, Rev. Mod. Phys. 45 (1973) 111.
- M. Gryzinski, Phys. Rev. 138, A322 (1965).
- W. D. Hamilton, "The Electromagnetic Interaction in Nuclear Spectroscopy", North-Holland (1975).
- J. M. Hansteen, Advances in Atomic and Molecular Physics 11 (1975) 299.
- K. Helfrich and H. Hartmann, Theoret. Chim. Acta 16 (1970) 263.
- F. Hopkins, A. Little, N. Cue and V. Dutkiewicz, Phys. Rev. Lett. 37 (1976) 1100.
- J. D. Jackson, Classical Electrodynamics (Wiley, Int. Science) 1962.
- Q. C. Kessel and B. Fastrup, Case Studies in Atomic Physics 3 (1973) 137.
- W. N. Lennard, I. V. Mitchell and J. S. Forster, Progress Report, Chemistry Branch, AECL-5808, 1977a.
- W. N. Lennard, I. V. Mitchell, J. S. Forster and D. Phillips, J. Phys. B: Atm. Molec. Phys. 10 (1977b) 2199.
- R. D. Levine, B. R. Johnson and R. B. Bernstein, J. Chem. Phys. 50 (1969) 1694.
- W. Lichten, Phys. Rev. 164 (1967) 131.
- J. R. MacDonald, M. D. Brown and T. Chiao, Phys. Rev. Lett. 30 (1973) 471.
- J. H. Macek and J. S. Briggs, J. Phys. B: Atom. Molec. Phys. 6 (1973) 841.

- J. H. Macek and J. S. Briggs, *J. Phys.* B7 (1974) 1312.
- D. H. Madison and E. Merzbacher, in *Atomic Inner-Shell Processes*, ed. B. Craseman (1975) 1.
- James H. McGuire and Patrick Richard, *Phys. Rev.* A8 (1973) 1374.
- E. Merzbacher and H. W. Lewis, X-ray Production by Heavy Charged Particles. In: *Encyclopedia of Physics*, ed. S. Flügge, Vol. 34 (Springer-Verlag, Berlin 1958) pp. 166-192.
- W. E. Meyerhof, *Phys. Rev. Lett.* 31 (1973) 1341.
- W.E. Meyerhof, T.K. Saylor, S.M. Lazarus, W.A. Little, B.B. Triplett and L.F. Chase Jr., *Phys. Rev. Lett.* 30 (1973) 1279.
- W. E. Meyerhof, *Science* 193 (1976) 839.
- W. E. Meyerhof, R. Anholt and T. K. Saylor, *Phys. Rev.* A18 (1977) 169.
- W. E. Meyerhof and Knud Taulbjerg, *Ann. Rev. Nuc. Sci.* 27 (1977) 279.
- P. H. Mokler, H. J. Stein and P. Armbruster, *Phys. Rev. Lett.* 29 (1972) 827.
- B. Müller, *Ann. Rev. Nuc. Sci.* 26 (1976) 351.
- B. Müller and W. Greiner, *Phys. Rev. Lett.* 33 (1974) 469.
- H. J. Nagy, G. Schupp and R. R. Hurst, *Phys. Rev.* C11 (1975) 205.
- L. C. Northcliffe and R. F. Schilling, *Nuc. Data Tables* 7 (1970) 233.
- David K. Olsen and C. Fred Moore, *Phys. Rev. Lett.* 33 (1974) 194.
- P. Richard in "Proceedings of the International Conference on Inner Shell Ionization Phenomena and Future Applications, Atlanta, Georgia, 1972", edited by R. H. Fink et al., CONF-72040 (U.S. Atomic Energy Commission, Oak Ridge, Tenn. 1973) p. 169.
- P. Richard, In: *Atomic Inner-Shell Processes*, ed. by B. Craseman (1975) 73.
- Patrick Richard, W. Hodge and C. Fred Moore, *Phys. Rev. Lett.* 29 (1972) 393.
- M. E. Rudd, D. Gregoire and J. B. Crooks, *Phys. Rev.* A3 (1971) 1635.

- A. Russek, Phys. Rev. A4 (1971) 635.
- F. W. Saris, Physica 52 (1971) 290.
- F. W. Saris, W. F. Van der Weg, H. Tawara and R. Laubert, Phys. Rev. Lett. 28 (1972) 717.
- H.W. Schnopper, H.-D. Betz, J.P. Delvaille, K. Kalata, A.R. Sohval, K.W. Jones and H.E. Wegner, Phys. Rev. Lett. 29 (1972) 898.
- J. H. Scofield, At. Data Nucl. Data Tables 14 (1974) 121.
- H. J. Specht, Z. Phys. 185 (1965) 301.
- H. J. Stein, H. O. Lutz, R. H. Mokler and P. Armbruster, Phys. Rev. A5 (1972) 2126.
- Knud Taulbjerg, J. S. Briggs and Jorgen Vaaben, J. Phys. B: Atom. Molec. Phys. 9, (1976) 1351.
- C. W. E. van Eijk and J. Wijnhorst, Phys. Rev. C15 (1977) 1068.
- J. von Neumann and E. P. Wigner, Z. Physik 30 (1929) 467.
- W. Wölfi, Ch. Stoller, G. Bonani, M. Suter and M. Stöckli, Phys. Rev. Lett. 35 (1975) 656.